

©Copyright 2017

Aaron N. Parks

# Employing Ambient RF Energy in Connected Devices

Aaron N. Parks

A dissertation  
submitted in partial fulfillment of the  
requirements for the degree of

Doctor of Philosophy

University of Washington

2017

Reading Committee:

Joshua R. Smith, Chair

Shyam Gollakota

Eric Klavins

Program Authorized to Offer Degree:  
UW Electrical Engineering

University of Washington

## Abstract

Employing Ambient RF Energy in Connected Devices

Aaron N. Parks

Chair of the Supervisory Committee:

Professor Joshua R. Smith

Department of Computer Science and Engineering, Department of Electrical Engineering

Pervasive connectivity is stunted by the requirement for batteries. RF energy harvesting is a compelling solution to this problem. However, the fundamental energy requirements of wireless communication limit the means for connectivity in these highly energy constrained RF harvesting devices. Further, variation in power availability for conventional RF harvesters, which target single fixed spectral bands, severely limits the area in which they can be applied.

Ambient bacskcatter addresses communication energy requirements by employing ambient RF energy in another way: devices perform modulated scattering of ambient RF to transmit information. This allows RF harvesting ambient backscatter devices to communicate with far less power than those using conventional radio, partially closing the gap between the power requirements of a connected device and the power harvesting capabilities of an ambient harvester.

Multiband RF harvesting addresses single-source energy availability issues by allowing an ambient harvesting node to gather energy on multiple bands at once, summing power efficiently from multiple ambient sources. A parallel method for resolving single-source fading issues in ambient backscatter is wideband ambient backscatter, in which a transmitter backscatters energy across an extremely wide bandwidth, allowing any signal in that entire band to be a host for backscatter communication.

The overall motivation of this work is to explore ways in which ambient RF can be practically employed in connected devices to prolong operating life, or even to allow batteryless operation.

## TABLE OF CONTENTS

	Page
List of Figures . . . . .	iv
Chapter 1: Introduction . . . . .	1
1.1 Ambient harvesting power supplies . . . . .	2
1.2 Power requirements of connected devices . . . . .	2
1.3 Where CMOS scaling doesn't help . . . . .	3
Chapter 2: Ambient RF Energy Harvesting . . . . .	5
2.1 Multiband RF harvesting . . . . .	6
2.2 Design of a Multiband Harvester . . . . .	8
2.2.1 Two multiband harvesting paradigms . . . . .	9
2.3 Design strategies for a multiband harvester . . . . .	10
2.3.1 Tuning . . . . .	11
2.3.2 Overcoming impedance matching limits . . . . .	12
2.3.3 Band power summation strategies . . . . .	13
2.3.4 Full shortcut diode network . . . . .	14
2.3.5 Simplified shortcut diode network . . . . .	16
2.3.6 Intelligent shortcut switching summation network . . . . .	16
2.3.7 Scaling considerations . . . . .	16
2.4 Simulating the Multiband Harvester . . . . .	17
2.4.1 Single-tone response . . . . .	18
2.4.2 Simulating power combination methods . . . . .	18
2.4.3 Analysis of power combination results . . . . .	21
2.5 Hardware Prototype: Design and Characterization . . . . .	22
2.5.1 Tuning the prototype . . . . .	22
2.5.2 Single-tone response . . . . .	23

2.5.3	Multi-excitation response . . . . .	25
2.5.4	In the wild . . . . .	25
2.6	Conclusions on Multiband Harvesting . . . . .	26
Chapter 3: Narrowband Ambient Backscatter . . . . .		28
3.1	Backscatter background . . . . .	28
3.2	Design of an ambient backscatter system . . . . .	29
3.2.1	Design of an ambient backscatter transmitter . . . . .	32
3.2.2	Ambient Backscattering Receiver . . . . .	33
3.3	Network Stack Design . . . . .	39
3.3.1	Physical Layer . . . . .	39
3.3.2	Link Layer . . . . .	41
3.4	A prototype ambient backscatter communicator . . . . .	41
3.5	Improving rate and range of ambient backscatter . . . . .	44
3.5.1	Leveraging system properties with $\mu$ MO . . . . .	45
3.5.2	Applying coding with $\mu$ Code . . . . .	46
Chapter 4: Wideband Ambient Backscatter . . . . .		52
4.1	Challenges and Goals . . . . .	52
4.1.1	Making use of all bands . . . . .	53
4.1.2	A First Approach . . . . .	54
4.1.3	Wideband Ambient Backscatter . . . . .	57
4.2	Design . . . . .	58
4.2.1	Transmitter Design . . . . .	59
4.2.2	Transmit antenna . . . . .	60
4.2.3	Receiver Design . . . . .	60
4.2.4	Scanning algorithm . . . . .	61
4.3	Modulation and Protocol . . . . .	62
4.3.1	Frequency plan . . . . .	62
4.3.2	Coding and Packet Structure . . . . .	64
4.3.3	Multi-user Capability . . . . .	65
4.4	Prototype implementation . . . . .	66
4.5	Experimental results . . . . .	70

4.5.1	Backscatter Capability . . . . .	70
4.5.2	Communication Performance . . . . .	71
4.5.3	Frequency Agility . . . . .	73
4.5.4	Quality of Service Testing for an Indoor Application . . . . .	76
4.5.5	Quality of Service Testing for an Outdoor Application . . . . .	78
4.5.6	Power Consumption of Tag . . . . .	79
4.5.7	Notes on Computational Burden of Receiver . . . . .	80
Chapter 5:	Prior Art . . . . .	81
5.1	Wideband / Multiband RF Energy Harvesting and Scavenging . . . . .	81
5.2	Communication by Backscatter Modulation . . . . .	82
5.2.1	Systems using Backscatter of Intentional Sources . . . . .	82
5.2.2	Systems using Backscatter of Ambient Sources . . . . .	83
5.2.3	Passive Tag-to-Tag Communication . . . . .	84
5.2.4	Subcarrier Modulated Backscastter . . . . .	85
Chapter 6:	Summary and Conclusion . . . . .	87
Bibliography	. . . . .	88

## LIST OF FIGURES

Figure Number	Page
2.1 A single-band harvester cannot efficiently collect energy over a large bandwidth. The proposed multiband harvester aims to divide and conquer an arbitrarily large bandwidth for efficient harvesting. . . . .	7
2.2 The topology of the proposed multiband harvester. A single wideband antenna is used, in contrast to other work. Bands are spaced geometrically with a frequency ratio R[34]. . . . .	9
2.3 One band in the proposed multiband harvester. Diode summation network is omitted for clarity. The trunk node is connected to the antenna in the full system[34]. . . . .	10
2.4 Four methods of serially combining power from multiple bands in a multiband RF harvester: (a) is the naive implementation involving simple serial combination. (b) adds implements the full diode summation network described in[34]. (c) simplifies the summation network to only first-tier shortcut diodes. (d) intelligently bypasses unexcited harvesters with normally-open switches. . . .	15
2.5 An example of the diode summation network, shown here for a 3-band harvester. The output voltage will be the global sum of the band outputs, less a small number of diode drops. . . . .	15
2.6 Control logic flowchart for implementing the intelligent summation network. Each loop iteration involves testing and updating only one switch, as this requires minimal energy and therefore a smaller reservoir of stored charge[31]. .	17
2.7 The RF-DC conversion efficiency of the simulated 8-band harvester, including the diode summation network. Design frequencies for each band are shown. .	19
2.8 Two multiband harvester prototypes were constructed: A 2-band harvester (a), and a 5-band harvester with diode summation network (b). The 5-band prototype measures 1.5 by 1.2 inches. . . . .	23
2.9 S11 (reflected power at RF port) and RF-DC conversion efficiency over the operating band for both the 2-band harvester (a) and 5-band harvester (b), for a -10 dBm test power and a 100 k $\Omega$ load. . . . .	24

2.10	Measured RF-DC conversion efficiency for the two-band prototype as a function of input power at both design frequencies. A 100 k $\Omega$ load was used. . . . .	24
2.11	The 5-band harvester prototype connected to a log-periodic antenna spanning 400-900 MHz. . . . .	26
3.1	<b>Ambient Backscatter:</b> Communication between two battery-free devices. One such device, Alice, can backscatter ambient signals that can be decoded by other ambient backscatter devices. To legacy receivers, this signal is simply an additional source of multi-path, and they can still decode the original transmission. . . . .	30
3.2	Comparison of the incident signal on a backscattering transmitter's antenna in both (a), ambient backscatter, and (b), conventional RFID. . . . .	34
3.3	Comparison of backscattered signal received both with (b) and without (a) averaging. . . . .	36
3.4	<b>Circuit Diagram for the Demodulator:</b> The demodulator has two stages: an envelope detection and averaging stage that produces an average envelope of the signal, and a compute-threshold stage that compares the averaged signal with a threshold value computed by taking a longer-term average of the signal.	37
3.5	<b>Packet Format:</b> Each packet starts with an alternating sequence of '1's and '0's followed by a preamble that is used by the receiver to detect packets. The preamble is followed by a header and then the data, which both include CRCs used to detect bit errors. . . . .	41
3.6	<b>Prototype:</b> A photo of our prototype PCB that can harvest, transmit and receive without needing a battery or powered reader. It also includes touch sensors (the A, B and C buttons), and LEDs (placed near the two arrows) that operate using harvested energy and can be programmed by an onboard microcontroller. . . . .	42
3.7	A prototype of the “turbocharged” ambient backscatter system, which integrates both $\mu$ mo and $\mu$ code in a single design. It can operate using both RFID and TV transmissions[32]. . . . .	45
3.8	<b><math>\mu</math>mo Decoding.</b> The two-antenna device, Alice, can decode Bob's backscattered information by separating the direct TV transmissions from the backscattered signals. $\mu$ mo achieves this operation with neither channel estimation nor digital computation. . . . .	47
3.9	$\mu$ mo on actual signals. It is difficult to see the backscattered bits on the received signals at the two receiver antennas. Performing the division between the received signals on the two antennas, reveals the backscattered bits[32]. .	48

3.10	<b><math>\mu</math>mo hardware design.</b> $\mu$ mo performs the required computation using analog components. Specifically, $\mu$ mo’s hardware has three main components: an envelope detector that removes the carrier frequency (e.g., 539 MHz), an analog division circuit that divides the received signal on the two antennas, and finally a thresholding circuit that outputs the 0 and 1 bits. . . . .	49
3.11	<b><math>\mu</math>code hardware design.</b> Our hardware design performs the decoding operations using analog components, without the need for ADCs. The hardware system has three main components: I/Q correlation circuits that compute $ I $ and $ Q $ , a summation circuit that computes $ I  +  Q $ , and finally a thresholding circuit that outputs 0 and 1 bits. . . . .	50
4.1	To achieve frequency diversity, an ambient backscatter device must be able to re-radiate multiple bands simultaneously. A receiver makes intelligent decisions about which bands to listen for. . . . .	53
4.2	A multiband ambient backscatter prototype . . . . .	55
4.3	An indication of how well isolated transmit bands are from each other in a five-band multiband ambient backscatter prototype. . . . .	56
4.4	The complementary transmit and receive architectures for the proposed wideband ambient backscatter system. . . . .	59
4.5	Frequency plan for subcarrier-offset wideband ambient backscatter, showing the original host signal and the re-radiated signal produced by the tag. . . .	64
4.6	Prototype of the wideband ambient backscatter transmitter. The antenna used is a compact, fairly low efficiency monopole designed for reception of TV signals in the 400-900 MHz range. In our experiments this antenna responds sufficiently down to around 100 MHz. The tag itself is composed simply of a TI MSP430F5310, an HMC550A wideband RF switch, and a 20mm coin cell battery. . . . .	68
4.7	This popular and inexpensive (about 20 US dollars) implementation of the RTL-SDR software defined radio is used in all experiments. This radio is capable of tuning across a range of 30 MHz to 1.3 GHz, and are thus well suited to pick up re-radiated energy from the tag in FM radio bands, TV bands, at frequencies used for industrial / scientific / medical applications, and cellular base station and mobile transceiver transmission frequencies. The ADC resolution of the radio is 8 bits, and the sampling rate may be varied from 1 to 3 MHz. . . . .	69

4.8	Graphical version of the gnuradio flowgraph implementing the correlating receiver. A matched filter is used to identify the presence of the PN sequence in the input signal. The Abcrx block is a custom out-of-tree module which does bit detection, passing detected bits to a python program which decodes packets and manages frequency scanning. . . . .	69
4.9	Measured real and reactive components of impedance at tag port, from 1MHz to 6GHz, for both open and short states. The heavy blue line shows the absolute contrast (vector distance) between open and short states. . . . .	70
4.10	Power spectral density in the 50 MHz to 1 GHz range for the two primary indoor and outdoor test locations, within several hundred meters of each other. Note that, in general, the outdoor location experiences much higher ambient power availability. . . . .	72
4.11	PER as a function of range for an outdoor scenario with low incident power at ground level, with several traces representing different receive frequencies.	72
4.12	The 6th floor balcony location used in frequency agility testing. . . . .	73
4.13	Tag and receiver were placed a varying distance apart in an elevated outdoor location, and the automated frequency selection algorithm was allowed to determine a suitable operating frequency at each location. . . . .	74
4.14	Test setup for indoor quality-of-service testing, with antennas separated by 2 ft on a rolling cart. . . . .	76
4.15	Quality of Service Testing across six floors of an office building, including two subterranean basement floors. Transmitter and receiver were placed at a fixed separation distance of 2 ft at each test location. Link frequency was 1 kbps for each test, with a PN sequence length of 63 and a subcarrier frequency offset of 10 MHz. . . . .	77
4.16	Cumulative distribution function of packet error rate across 74 test locations in an office building . . . . .	78
4.17	Quality of service testing across 87 outdoor locations in various neighborhoods of Seattle, Washington. TX and RX were placed at a 6ft separation on the roof of a car and driven to each test location. . . . .	79
4.18	Cumulative distribution function of packet error rate across 87 outdoor test locations with a 6 ft TX-RX spacing . . . . .	80

## **ACKNOWLEDGMENTS**

This work is the product of many individuals. Thanks to my advisor, Prof. Josh Smith, for his support on so many fronts and whose technical know-how and creative insights have been invaluable. A special thanks to Dr. Alanson Sample, whose technical and career mentorship helped me tremendously throughout my early graduate school career, and whose own projects inspired much of my work. Also, thanks to all the present and former UW Sensor Systems lab group members who have contributed to the projects I present here and without whom this wouldn't have been nearly as much fun.

## Chapter 1

# INTRODUCTION

Across industries and in academic labs, engineers and business people have long been investigating the technological and commercial potential of small, inexpensive connected devices. These devices, which perform sensing, computation, communication, and actuation functions, can now be seen in every venue from retail environments (in the form of RFID tagging and electronic shelf labels) to agriculture (in the form of micro-management of crops through soil sensing).

The increasingly pervasive ecosystem of connected electronics has encountered a major problem: massive proliferation of battery-operated devices isn't sustainable. Rooftop sensors monitoring the air quality or crop micro-management solutions, needing a battery replacement every few years, will be subject to the maintenance costs and effort associated with this periodic battery replacement, while deeply embedded devices such as structural health monitors strapped to I-beams in a skyscraper will be doomed to eventually run out of energy and cease functioning. In typical sensing nodes, battery life is limited from several months to around 10 years of use, while all the other solid state components making up such devices can last many decades.

To realize the vision of pervasive connectivity without compromise, a solution which eliminates the local expendable energy source is needed. The resulting system, having no reliance on an onboard energy supply, will not be subject to the same lifespan constraints or maintenance requirements as conventional systems.

Deeply embedded systems in particular will benefit from eliminating batteries. There are many potential applications of connected devices which the industry has not pursued, simply because they aren't worth the effort required to replace batteries. As an example, building

materials or wallpaper sold with embedded devices performing proximity sensing could be used as part of security system or to track occupancy of a large structure. While this is a compelling use case and a logical progression of existing methods, the requirement to replace batteries, even once per decade, would render the system's maintenance too expensive to justify its use over existing methods.

### ***1.1 Ambient harvesting power supplies***

Ambient radio frequency harvesting provides an opportunity for small scale, low power devices to derive their power requirements from energy already present in their environment. The possible batteryless or “energy-neutral” future that this implies has been a motivator for work in ambient energy harvesting over the past decade. However, there is currently a large gap between the power supply requirements of even the simplest devices, and the availability of ambient radio frequency energy.

This work aims to close the gap between what is achievable by an ambient harvesting power supply, and the power requirements of simple connected devices. The result would be a new state of the art in which ambient harvesting is of practical value. A two-tiered approach to doing this involves both improving the capabilities of the ambient harvesting supply as well as optimizing the power supply requirements of the connected device such that it better complements the capabilities of the ambient harvesting supply.

### ***1.2 Power requirements of connected devices***

The tasks performed by a connected device fall into one of four categories:

- **Sensing** Environmental quantities are recorded
- **Computation** Signal processing and decision making is done
- **Communication** Data is transmitted to a peer or external sink
- **Actuation** Environmental changes are introduced

One can consider the power budget of a connected device as a product of the energy required for each task the device is capable of performing with the frequency at which each task is typically performed. Some devices, such as a smoke alarm, are complicating in that they on average have a very low typical power requirement, but that they also must be able to consume large amounts of power when required. The smoke alarm can monitor a home for ten years without battery replacement, but when smoke is detected and the alarm is sounding the battery will be depleted within hours, as the power requirement for actuating the alarm is many orders of magnitude higher than that required for the sensing task.

Many connected devices are required to stay in frequent contact with the outside world. Because radio communication costs significant energy, it is often the case that the power budget of a connected device is dominated by the power required for communication.

### **1.3 Where CMOS scaling doesn't help**

While CMOS technology trends continue to bring down the power requirements of pure digital logic[23], the circuitry on the fringes of the connected system still requires significant power. Fortunately, sensing devices have also trended towards very low power requirements; for instance, the average energy required to sample a 3-axis accelerometer has decreased by a factor a 100 over a span of several years, based on datasheet power numbers from a major sensor manufacturers[4]. Additionally, actuation has in many instances trended towards lower requirements: Incandescent lamps were replaced by LEDs, which grow increasingly efficient each year; backlit LCD displays are now being replaced in many cases by reflective type displays such as the Qualcomm Mirasol system and E-ink's electrophoretic displays.

But the activity which has long dominated the power budget of many connected devices is still communication, and here there has been a fundamental minimum energy requirement, as implied by Shannon's channel capacity theorem, to achieve a given rate of transmission over a given distance in a given noisy environment. Because the radio must emit some power in order to produce a detectable change at a distant receiver, the power requirements of the radio can never fall below this emitted power.

While sensing, computation, and actuation tasks are still far from their theoretical minimum power requirements, the power-hungry communication systems of connected devices are only a factor of two or so away from their theoretical minimum power requirements. This begs the question: What will happen to the power trend for connected devices when the communication system can't be further optimized? To reduce transmission requirements, data may be compressed prior to transmission (at a computational cost) and decompressed at the receiver, but this also is a fundamentally limited process and can't achieve the orders-of-magnitude gains that other tasks may well experience in the coming years.

The answer may be found in exploring a new paradigm for wireless communication, which is what this work aims to do. In this paradigm, existing signals emitted by external (unrelated) radio transmitters are leveraged as a communication channel for power-constrained connected devices. The existing signals are exploited for this purpose by means of the connected device modulating its reflection, or scattering, of those signals.

### *Dissertation outline*

The remainder of this dissertation will describe the steps taken towards employing existing ambient energy to reduce the power requirements of connected devices. Two related areas are covered: Ambient RF energy harvesting (Chapter 2), and Ambient backscatter communication (Chapter 3). These two techniques employ ambient RF energy on a connected device in complementary ways. Both single-frequency and multi-frequency harvesting will be presented, along with results of prototype implementations of both. Ambient backscatter, a new design primitive which employs ambient signals as a medium over which communication can take place, is explored in both single-band and wideband implementations.

## Chapter 2

### AMBIENT RF ENERGY HARVESTING

“Wild” ambient RF energy sources exist in the built environment. In general, these signals are not intended to be used as a power source, but instead are simply carrying information. Nevertheless, power can be captured from these ambient signaling sources and converted to DC for use by connected devices. These sources of ambient RF energy include:

- Broadcast sources such as TV and radio.
- Directed multiuser sources such as cellular base station transceivers and Wi-Fi.
- Directed or undirected peer to peer wireless links such as Bluetooth, ZigBee, and wireless backhauls.

RF harvesting is done by impedance matching an antenna to a rectifier, which then performs RF-DC conversion. The resulting DC is then often further processed by a voltage conversion stage, and regulated for use at the load.

Impedance matching constraints between the antenna and rectifier create a fundamental limitation in the bandwidth across which an RF harvester can efficiently capture energy. While one would like to capture energy across any available band, this is not a practical possibility. As described by Fano in a seminal 1948 paper[14], a load can either be well matched to a source over a narrow band, or poorly matched over a wideband, but cannot be well matched across a wide band.

However, ambient signals are not individually wideband in nature, and thus a wideband harvester is not what is required. Instead, this work argues that what is needed is a multiband harvester, efficient at some number of discrete frequencies. While the overall matching

bandwidth of such a harvester may not be far different from a single-band, such a harvester can capture efficiently several narrowband ambient signals which may be very far from each other in frequency. The following section describes a multiband harvesting system that has been developed.

## **2.1 Multiband RF harvesting**

Ambient radio harvesting is a promising approach to powering battery-free sensing, computing, and communication devices[41, 33, 42]. The vanishingly small amount of power now required by modern microelectronics[23, 45] make ambient radio harvesting an increasingly viable power supply option. Compared to solar power, ambient RF has the advantage of being available at night, and is attractive from an industrial design perspective: the antennas already used in mobile devices for communication purposes can potentially become a power source, without requiring any changes to the form factor or appearance of the device.

However, there still exist crippling roadblocks preventing widespread adoption of ambient RF harvesting as a power source. Conventional RF harvesting methods are only capable of extracting power from a narrow spectral band. The supply will cease to provide power when its particular source band is not available, either due to geographical fluctuations in spectral occupation, occlusion and shielding (e.g., from the walls of a building), or simply from multipath fading of the ambient signal. When starved of its energy source the device must cease to operate, limiting the application space mostly to a small geographical area with line-of-sight to an ambient radio source of interest.

Some work has been done on wideband harvesting[15], tunable harvesting[44], and multi-band harvesting[21, 30]. While wideband harvesting can capture energy across a large swath of spectrum, it typically results in very low efficiency at any particular source frequency as the quality of the impedance match between the antenna and single rectifier must reduce as the bandwidth increases[14]. Tunable harvesting allows a system to dynamically select a band of interest based on spectral availability, and therefore promises to be able to provide efficient rectification of signals from a single source, regardless of the frequency of that

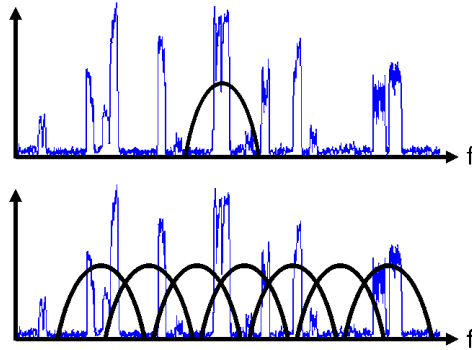


Figure 2.1: A single-band harvester cannot efficiently collect energy over a large bandwidth. The proposed multiband harvester aims to divide and conquer an arbitrarily large bandwidth for efficient harvesting.

source. However, tunable harvesters in battery free systems will require solving the very difficult bootstrapping problem to allow the system to cold-start, and also will ignore energy outside the band to which they are tuned.

Multiband harvesting involves building an array of harvesters, each tuned to an adjacent but orthogonal frequency band, and has the benefit of being able to capture power efficiently from multiple bands at once[34]. Existing work on multiband harvesting typically makes use of multiple antennas, each tuned to a band of interest, and each feeding an independent rectifier through a tuned matching circuit[21]. In existing work, the DC output from each rectifier is usually then serially combined to produce a voltage sum which becomes the multiband harvester output.

This work aims to produce a more practical multiband harvester, which does not require multiple antennas. A single wideband antenna feeds a trunk node which is electrically split into independent branches by orthogonally tuned band-pass filters. Each branch is then impedance matched to an independent rectifier, and the rectifier outputs are summed at DC by a novel method.

In the remainder of this section, the novel single-antenna multiband harvester is presented

and design choices are described and defended[34]. A strategy is presented for computing and optimizing bandpass filter and impedance matching values to produce an efficient system. A method is presented for efficiently summing many independent rectifier outputs using a network of diodes. Simulations are performed for an eight-band harvester and used to explore the design tradeoffs for this system, and both a two-band and a five-band prototype are developed and characterized.

## **2.2 Design of a Multiband Harvester**

The multiband charge pump topology presented here is based on the Dickson charge pump, a circuit commonly used in RF-DC conversion which provides both rectification and impedance transformation[11]. The unique aspect of the design presented here is the ability to capture power from multiple bands, and combine this power in an optimal way for any combination of excited bands. Figure 2.2 illustrates the architecture of the proposed method and Figure 2.3 shows the circuit topology for a single band of the harvester.

Our multiband harvester covers N adjacent frequency bands, each with an M stage Dickson charge pump providing rectification and voltage multiplication. The number of bands (N), the geometric spacing of the band frequencies ( $R = \frac{f_n}{f_{n-1}}$ ), and the number of stages for each band are all key parameters of the design space.

One departure from existing work is that this parallel harvester topology is designed to provide a good match to one single-port antenna at multiple bands, whereas most published multiband harvesting topologies make use of multiple antennas, each covering a particular band of interest[21], or make use of dual-band antennas with multiple ports and a single rectifier[30]. Therefore, in contrast to existing work, this system can scale to a large number of frequency bands with no additional antennas or antenna ports required. We imagine this system being useful as a universal solution for RF energy harvesting implementations, especially if scaled to a large number of frequency bands (and therefore acting as an efficient harvester across a very wide bandwidth). With such a universal harvesting solution, the choice of antenna then becomes the sole responsibility of the application developer.

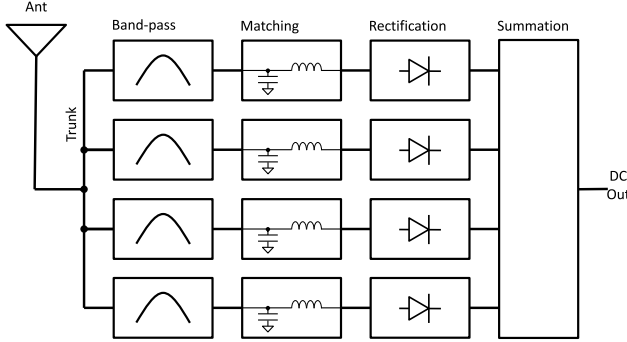


Figure 2.2: The topology of the proposed multiband harvester. A single wideband antenna is used, in contrast to other work. Bands are spaced geometrically with a frequency ratio  $R$ [34].

Another departure from existing work is in the method of combination of the harvester DC output paths. Most existing multi-harvester systems use a simple serial connection between independent rectifiers, a topology which, in the context of multiband harvesting, only provides high efficiency in the case where all bands are excited. If one or more bands in such a serially connected system are not excited, the diode drops in the unexcited bands' charge pumps must be overcome by the other bands, resulting in a major efficiency degradation. Our solution is to use “shortcut” diodes to bypass the bands which are not active, thereby allowing an automatic optimal configuration to be achieved in summing the voltages produced by each band rectifier. These shortcut diodes ideally have both low threshold and low leakage, attributes which are very achievable as they will be operating at DC.

### 2.2.1 Two multiband harvesting paradigms

We envision that frequency band selection for the multiband harvester may follow one of two possible paradigms, depending on intended application:

1. A multi-protocol arrangement targeting several commonly used bands. For instance, 433 MHz, 915 MHz, and 2.45 GHz could be simultaneously targeted.

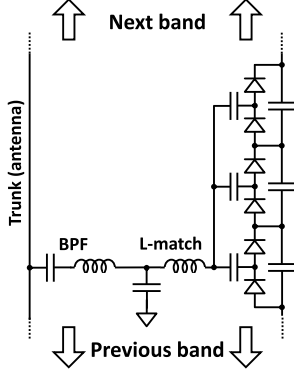


Figure 2.3: One band in the proposed multiband harvester. Diode summation network is omitted for clarity. The trunk node is connected to the antenna in the full system[34].

2. A tightly packed arrangement for efficient harvesting over a very wide bandwidth. This arrangement allows any number and placement of RF signals to be efficiently harvested, provided they are within the design bandwidth.

The first paradigm leverages knowledge of commonly occupied portions of the spectrum, which will be most likely to yield power. This method could achieve high practical efficiency with low complexity, as the number of target bands could be relatively small.

The second paradigm allows the harvester to capture energy at nearly any frequency in a large prescribed bandwidth (e.g., the 267-1350 MHz bandwidth targeted by our prototype). This has potential to become a universally applicable and future-proof method, as it doesn't rely on knowledge of commonly occupied bands, or on current details of regulatory spectral allocation.

### **2.3 Design strategies for a multiband harvester**

The multiband harvester consists of a single wideband antenna feeding an array of harvester bands, each of which is designed to target a particular frequency range. We select the center of this intended range and refer to this as the “design frequency” for each band. We have explored two challenges in implementation of such a harvester: Tuning strategies for

optimizing harvesting efficiency, and power combination strategies which allow simultaneous extraction of power from many bands.

### 2.3.1 Tuning

The tuning of the parallel-connected filtering and impedance matching networks which feed independent rectifiers is a very high dimensional problem and perhaps the most unique and interesting challenge in developing this particular multiband harvesting system.

In this work, we consider phrasing this tuning challenge as an optimization problem with a carefully designed cost function. The cost function used here is based on two main factors:

1. We aim to minimize reflected energy in matching the antenna to the trunk of the multiband harvesting network. In other words, the sum of S11 at each design frequency should be minimized.
2. We aim to minimize the impact of adjacent harvester branches on the impedance of the network at each band's design frequency. In other words, for each design frequency, the impedance of adjacent bands is maximized.

In our proposed optimization strategy, a weighted combination of the above terms could be minimized to select the bandpass filter and match network values for each band of the harvester.

The decision to minimize overall S11 at each design frequency while maximizing adjacent band impedance can be illustrated by considering a scenario in which only a single continuous wave is presented to the multiband harvester. If we simply minimize overall S11, the power of this continuous wave may end up distributed over several consecutive rectifiers, resulting in several very poorly excited rectifiers and therefore a very inefficient system. To also minimize the match quality of adjacent bands means that, instead of distributing this continuous wave's power, we focus this power on one rectifier and thereby maximize the efficiency of the system in harvesting that continuous wave signal.

Since most ambient or intentionally radiated signals are relatively narrow bandwidth compared to the overall scope of our harvester, most sources will excite only one of the bands of the harvester and therefore support the logic of this optimization strategy.

A heuristic for achieving these tuning goals involves making the simplifying assumption that the bandpass filter is a short when resonant and an open otherwise, and to design the matching network given this simplified model of the bandpass filter. The resulting match network values in this method are the same as those for a single-band harvester, and it is simply the addition of the bandpass filters which enables efficient multiband operation. We make use of this simplified method to tune the prototype harvesters in section 2.5.

A simple lumped element model of the harvester was developed in MATLAB. The model makes use of rectifier impedance measurements taken from actual prototypes; each rectifier in the multiband harvester must be characterized at each of the design frequencies in order to achieve a realistic model of the harvester. A simplified model of the antenna is used in which impedance is a constant  $50 \Omega$  across the entire band of interest, which allows for simplified experimentation. Although this will not accurately represent the frequency-dependent impedance of a real antenna, it's conceivable that in future work the antenna impedance could be measured across the operating bandwidth and used to better tune the system.

First approximations for the bandpass filter and L-match network values for each band are forward-computed by assuming each band is independent and simply selecting the values which achieve minimal  $S_{11}$ . This is a first guess, and could ultimately be used as the seed value for an optimizing search based on the strategy described above. The resulting match values would be bandpass and L-match network values which minimize overall  $S_{11}$  at each design frequency while minimizing interaction between adjacent bands, as described.

### *2.3.2 Overcoming impedance matching limits*

The Bode-Fano theorem describes the limits of impedance matching between a source and one complex load[14]. In conventional single-band RF harvesters or wideband harvesters, the

bandwidth over which the antenna can be well matched to a single rectifier will be limited, therefore placing an upper limit on the size of the band over which the RF-DC conversion will remain efficient.

We hypothesize that the multiband harvester topology presented herein may be able to circumvent the Bode-Fano limit by allowing the match to effectively be distributed across multiple loads.

There are at least two impedance interfaces in the multiband system that need to be well-matched for efficient RF-DC conversion at a given frequency. The first is the interface between the antenna port and the trunk node of the multiband harvester. The second is the interface between the trunk node and the load (rectifier) for each of the branches.

The Bode-Fano theorem only places a limit on match bandwidth for complex sources and/or loads. It will certainly model the limitations of the match between the trunk and the rectifier for each branch, since the rectifier impedance will always be complex. However, the antenna-to-trunk interface can be designed such that the impedance looking into each bandpass filter at its resonant frequency is real and matched to the antenna. Because the adjacent branch bandpass filters are assumed to have negligible admittance at the design frequency of any given band, they ideally will not contribute significantly to the impedance viewed from the trunk node at adjacent bands.

In summary, we hypothesize that each branch of the harvester will be Bode-Fano-constrained, but that the antenna-to-trunk match (and therefore the system as a whole) will not be constrained.

### *2.3.3 Band power summation strategies*

Most existing multiband systems simply serially combine the output of each band. This naive approach has a major flaw: low efficiency in most real-world use cases! Most existing systems are developed and tested under the assumption that all bands will be excited at all times, and in those cases may perform very efficiently. However, not all frequencies in the radio spectrum are inhabited in all locations and at all times. When one (or more) bands

in these systems remains unexcited, the diodes in the unexcited band's charge pump now represent an obstacle to current flow from the excited bands. These "dead weight" diodes can drop significant voltage and severely impact efficiency.

Serial summation topologies give the best voltage sensitivity, which is key when considering operating requirements of the load; a typical load will need significant developed voltage to operate. Even a DC-DC conversion stage will typically require hundreds of millivolts in order to bootstrap and begin moving charge[33].

In [34], we describe why a simple serial combination of RF harvesters hinders current flow when some bands are not excited. This turns out to be due to the impact of the unexcited bands' RF-DC conversion diodes; at low or zero excitation power the diodes cease to be a source of voltage and begin developing a voltage drop, therefore impeding the flow of current from serially-connected excited bands. Summation topologies which overcome this must allow current to divert *around* unexcited bands by providing a path of far lesser resistance. In effect, inactive bands must be shorted by some switching method.

Because it's difficult to produce semiconductor switches which are normally-closed with no supply voltage present, a harvester which is capable of cold-starting (starting with all circuit nodes at zero volts) cannot have normally-closed connections. This reinforces the decision to use a serial topology; normally-open switches can be used to short inactive bands and will also behave as open switches during a cold-start.

There are multiple ways to address the serial combination of bands which include unexcited bands. The following three methods for summation will be discussed in this work:

#### 2.3.4 Full shortcut diode network

The switches mentioned above for shorting unexcited bands can in fact be implemented by diodes. Shorting unexcited harvester bands simply requires an anti-parallel-connected diode which becomes forward-biased when the band output voltage is small and when other bands become active. Prior work[34] described a network of diodes for summation of power from multiple serially-connected bands, which ensures that each excited band is separated from

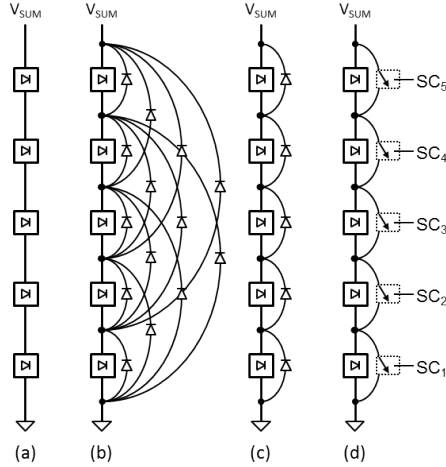


Figure 2.4: Four methods of serially combining power from multiple bands in a multiband RF harvester: (a) is the naive implementation involving simple serial combination. (b) adds implements the full diode summation network described in[34]. (c) simplifies the summation network to only first-tier shortcut diodes. (d) intelligently bypasses unexcited harvesters with normally-open switches.

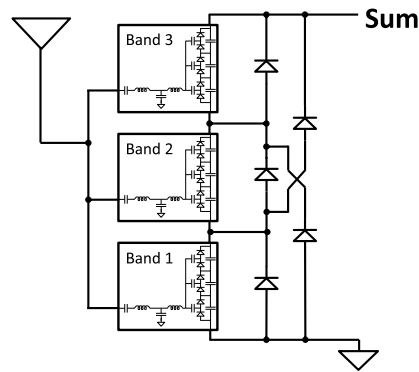


Figure 2.5: An example of the diode summation network, shown here for a 3-band harvester. The output voltage will be the global sum of the band outputs, less a small number of diode drops.

others by at most one diode drop. This network is shown in Figure 2.4 (b) and will be the first topology characterized.

### *2.3.5 Simplified shortcut diode network*

This work proposes a simplification of the full diode network, in which only the first level of shortcut diodes is implemented. This has the benefit of lower complexity and potentially lower sum leakage current in large band count multiband harvesters. This topology is shown in Figure 2.4 (c).

### *2.3.6 Intelligent shortcut switching summation network*

The final topology proposed in this work replaces diode switching with controlled analog switches, which are managed by a logic system[31]. The switches themselves are pictured in Figure 2.4 (d). A flow diagram for a logic system to control those switches is given in Figure 2.6.

### *2.3.7 Scaling considerations*

Scaling the multiband harvester to a large number of bands seems increasingly difficult for implementation with discrete components. As the number of bands increases, the component count also increases (including the shortcut network), and so the overall size of the multiband array becomes significant with respect to the wavelength and therefore the lumped modeling done here is not sufficient. Distributed modeling will likely be needed for multiband harvesters with a large band count, significantly increasing the complexity of modeling and the difficulty of tuning the harvester.

The frequency spacing between bands of the multiband harvester is a critical design parameter. Closely spaced bands exhibit more interaction and are therefore less efficient, particularly with the low Q bandpass filters achievable with discrete components. However, distantly placed bands can leave large gaps in spectral coverage, where RF-DC conversion

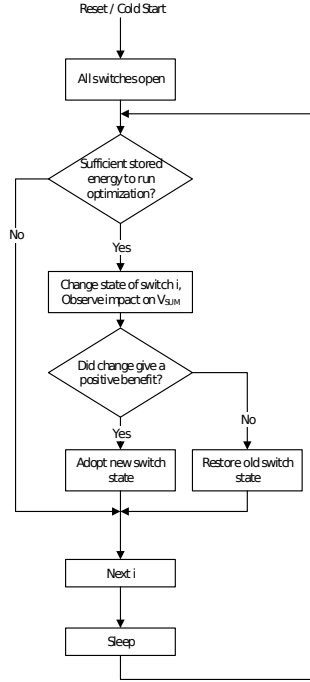


Figure 2.6: Control logic flowchart for implementing the intelligent summation network. Each loop iteration involves testing and updating only one switch, as this requires minimal energy and therefore a smaller reservoir of stored charge[31].

efficiency will be low. We hypothesize that there is an optimal frequency ratio between bands given a particular bandpass filter Q value, but exploring this tradeoff is outside the scope of this work.

## 2.4 Simulating the Multiband Harvester

To explore the feasibility of this multiband harvesting concept, a SPICE model of a multiband harvester was constructed and subjected to some virtual experimentation.

First, a single band model was constructed using Avago HSMS-285C diode models in a 3-stage Dickson charge pump arrangement. The impedance of the single band charge pump was measured at each of the design frequencies for the system. Eight bands in the UHF region of the spectrum were selected: 300 MHz, 356 MHz, 423 MHz, 503 MHz, 597 MHz, 709 MHz,

842 MHz, and 1 GHz. A first order LC bandpass filter was generated at each design frequency (with a Q of 5) and used to isolate the eight bands. A low-pass L-match network was then constructed for each band, to match the  $50\ \Omega$  source to the load impedance of each band's rectifier at its design frequency. All values were forward-computed based on initial simulated impedance measurements; no iteration was performed once initial component values had been selected.

A diode summation network was also constructed using the SPICE model for the SDM03U40 Schottky diode manufactured by Diodes, Inc., and used to sum the DC output power from each of the eight bands. The output of the summation network was connected to a  $100\ k\Omega$  load resistor to simulate a device being powered.

#### *2.4.1 Single-tone response*

Figure 2.7 shows the RF-DC conversion efficiency as a function of frequency for a single-tone excitation. The intended design frequencies align well with the conversion efficiency peaks, though there is significant variation in the conversion efficiency between bands. The fact that the outer bands are more efficient is a hint that a varying amount interaction between bands may be the cause of the efficiency variation. Bands near the center will always experience more interaction with adjacent bands than those near the outside of the targeted range.

#### *2.4.2 Simulating power combination methods*

Models of each of the three summation topologies were constructed. A 5-band harvester model was used as a source in a simulation testbench. The goal of modeling is to characterize the summation benefit of each method over a naive serial combination of DC harvester outputs as a function of the excitation state of the 5-band harvester.

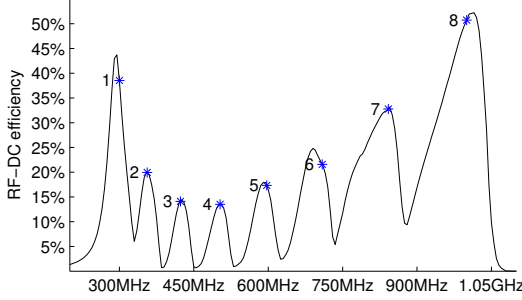


Figure 2.7: The RF-DC conversion efficiency of the simulated 8-band harvester, including the diode summation network. Design frequencies for each band are shown.

#### *Test setup: Multiexcitation testing*

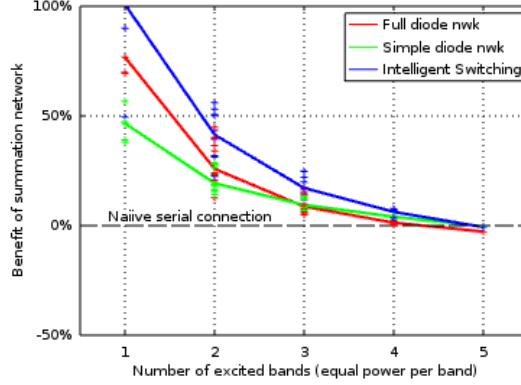
Two fixed-resistance loads were used in each test scenario,  $10\text{ k}\Omega$  and  $100\text{ k}\Omega$ , and represent typical  $\mu\text{W}$ -scale loads experienced in an energy harvesting device[24]. A load capacitance of  $10\text{ nF}$  was used.<sup>1</sup> Two excitation power levels were used in each test scenario, -10 dBm and -20 dBm. In the multiexcitation tests, each excited band for a particular test was subjected to this excitation power and the other frequency bands were left unexcited. Every possible permutation of excited bands was tested for each data set. For each data point in each set, a transient simulation was allowed to run until a stable output voltage was reached, and the power across the load was then computed.

Low forward voltage and low reverse saturation current both must be achieved for summation network diodes to have a positive benefit. In all tests the HSMS-282 Schottky barrier diodes were used for summation as they have very low advertised forward voltage while maintaining low reverse saturation current. The parameters of the diode models used in the diode summation network are given in Table 2.1.

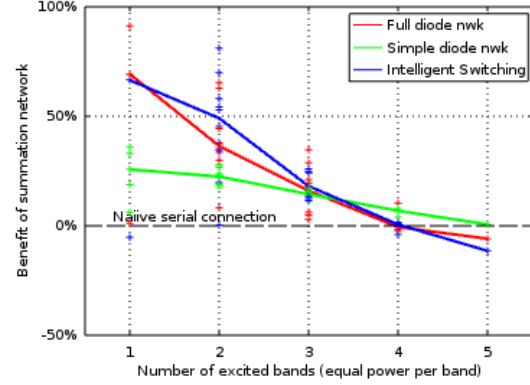
In the modeled intelligent switching network, bands left unexcited were bypassed by

---

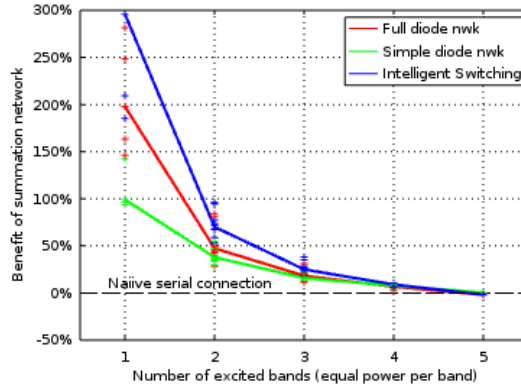
<sup>1</sup>Note that parasitic conductance in a storage capacitor is typically a source of quiescent current draw in such a system. The loads modeled herein are large enough to make it safe to neglect such parasitic conductance in most cases.



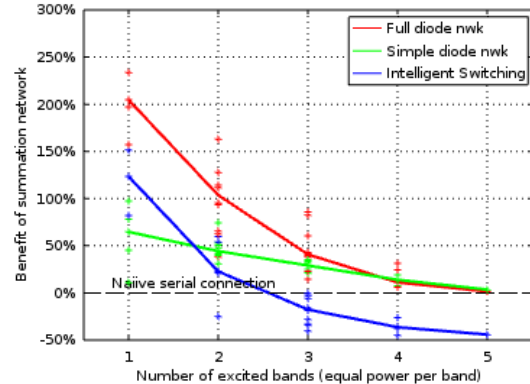
(a) Benefit of three summation networks with  $R_{LOAD} = 100 \text{ k}\Omega$ ,  $P_{RF} = -10 \text{ dBm}$  per band.



(b) Benefit of three summation networks with  $R_{LOAD} = 100 \text{ k}\Omega$ ,  $P_{RF} = -20 \text{ dBm}$  per band.



(c) Benefit of three summation networks with  $R_{LOAD} = 10 \text{ k}\Omega$ ,  $P_{RF} = -10 \text{ dBm}$  per band.



(d) Benefit of three summation networks with  $R_{LOAD} = 10 \text{ k}\Omega$ ,  $P_{RF} = -20 \text{ dBm}$  per band.

switches. The switch model used a  $50 \Omega$  'on' resistance and a  $10 \text{ M}\Omega$  'off' resistance, conservatively chosen values for low power analog switches such as the ADG802 operating at low voltages[2]. Switch power consumption for the ADG802 is under  $10 \text{ nW}$  per device. To estimate the overhead of the control logic, a TI MSP430G2553 microcontroller power consumption in low power mode (LPM3, with a crystal oscillator active) was assumed[5]<sup>2</sup>. The

<sup>2</sup>Though the microcontroller cannot actively control switches in low power mode, it can choose to spend the overwhelming majority of its time in this mode and therefore it's an acceptable approximation of power consumption.

total power consumption of switches and control logic is just under  $1 \mu\text{W}$ , and all results involving intelligent switching reflect this overhead.

#### 2.4.3 Analysis of power combination results

Figures 2.8(a), 2.8(b), 2.8(c), and 2.8(d) illustrate multiband harvester performance using each of the three summation methods from Figure 2.4 for two power levels and two values of load resistance. For each permutation of excited harvester bands, total power delivered to the specified load resistance was determined for each of the three summation topologies of Figures 2.4 (b),(c), and (d), and for the naive serial connection of Figure 2.4 (a). The solid line in each plot shows the median benefit of the summation network as a fractional power increase over the naive serial implementation, which is shown by the dotted black line.

It is observed that the diode summation network of Figure 2.4 (b) generally provides a benefit excepting the case in which all five bands are excited. The simple diode summation network of Figure 2.4 (c) also reliably provides a benefit, but in general is less beneficial than the full diode summation network.

The intelligent switching summation network, however, provides a strong benefit at higher input power (Figure 2.8(a) and 2.8(c)) but is less advantageous, and even becomes an impediment, as excitation power drops (especially Figure 2.8(d)). This decrease in efficacy with very low excitation power is a symptom of the power draw of the logic system for the intelligent switching network, and therefore is highly dependent on specific implementation.

Table 2.1: SPICE model for HSMS-282 diode used in serial summation

D( IS=4.8E-8, CJO=0.649E-12, VJ=.56 , BV=26.7, IBV=10E-4, EG=0.69 , N=1.067, RS=7.8 , XTI=2, M=0.5 )
---

## 2.5 Hardware Prototype: Design and Characterization

A 2-band and 5-band prototype are implemented with discrete components, as shown in Figure 2.8(e) and 2.8(f). The prototypes use 3 stage Dickson charge pumps in each band, use the described "shortcut" summation topology, and when the experiment requires they are connected to a wideband log-periodic antenna with a roughly 6 dBi gain. The two-band harvester design frequencies are 539 MHz and 915 MHz, and target an ambient television signal near our campus and an RFID reader, respectively. The five-band harvester design frequencies were chosen by selecting a fixed ratio of 1.5 between adjacent frequency bands, and are 267 MHz, 400 MHz, 600 MHz, 900 MHz, and 1.35 GHz.

Avago HSMS-285C Schottky diodes are used in the 3-stage RF-DC conversion charge pumps. The summation network makes use of low-threshold and low-leakage SDM03U40 diodes manufactured by Diodes, Inc.

### 2.5.1 Tuning the prototype

Tuning of the prototypes was accomplished by first treating each band independently prior to combining them in parallel. We first shorted the bandpass filter for each band in isolation, and iteratively searched for L-match network values which gave a good match for that band. Once a good match was accomplished with the bandpass filter shorted, we forward computed bandpass filter component values (using  $Q=1$ ). These filters were installed, and it was verified that the change in input impedance at the trunk node (for each design frequency) with the introduction of the filter was not significant. After performing the above steps for every band in isolation, all bands were installed and the overall behavior of the harvester could be observed. All iterative tuning was done at a test power of -10 dBm.

During the following tests to characterize the performance of the harvester, A  $100\text{ k}\Omega$  resistive load was placed at the output of the summation network.

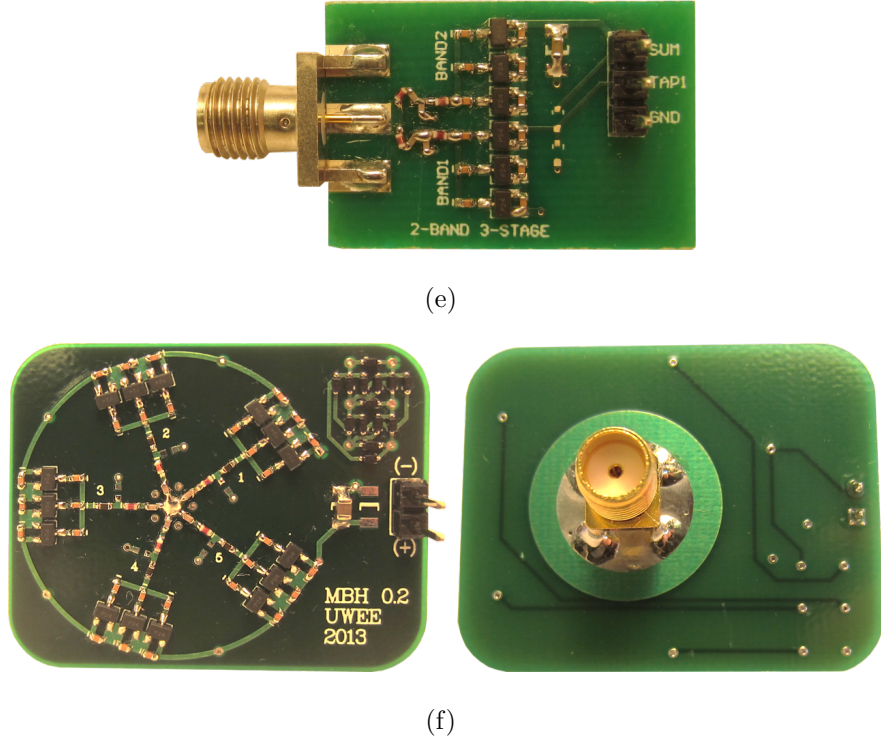


Figure 2.8: Two multiband harvester prototypes were constructed: A 2-band harvester (a), and a 5-band harvester with diode summation network (b). The 5-band prototype measures 1.5 by 1.2 inches.

### 2.5.2 Single-tone response

The 2-band and 5-band prototypes were first subjected to a single-tone excitation at a power level of -10 dBm ( $100 \mu\text{W}$ ), and the S11 (reflected power) and RF-DC conversion efficiency were measured. These single-tone results are shown in Figures 2.9(a) and 2.9(b).

We observe that, in this system, S11 is not a good predictor for RF-DC conversion efficiency. While the minimal S11 and maximal RF-DC efficiency points for the 2-band prototype matched well, the 5-band harvester did not exhibit the same correlation for every band. For instance, there were many spurious dips in the S11 which did not correspond to design frequencies, and for which conversion efficiency was very low. We also note that the peak efficiency decreased when moving from the 2-band to the 5-band system. We

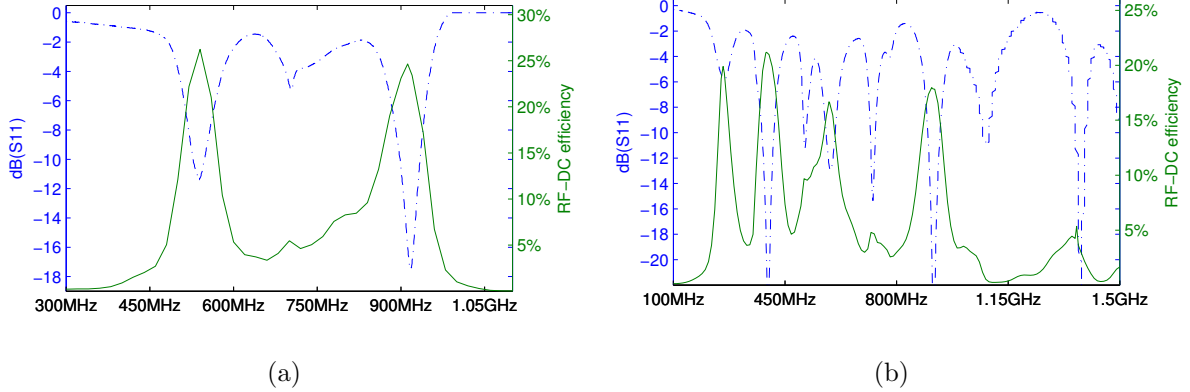


Figure 2.9: S11 (reflected power at RF port) and RF-DC conversion efficiency over the operating band for both the 2-band harvester (a) and 5-band harvester (b), for a -10 dBm test power and a  $100 \text{ k}\Omega$  load.

hypothesize that both of these effects are due to interaction between adjacent bands in the system, as the quality factor of the isolating bandpass filters was very low.

The fifth band exhibited a very poor RF-DC conversion efficiency, again seemingly in

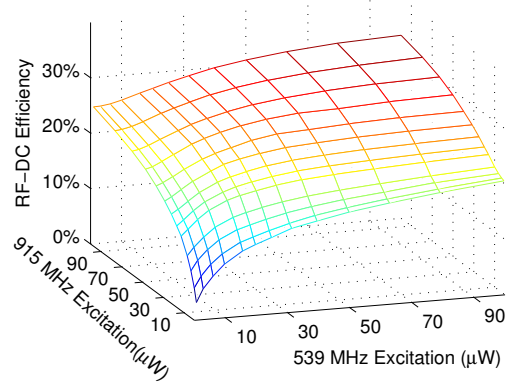


Figure 2.10: Measured RF-DC conversion efficiency for the two-band prototype as a function of input power at both design frequencies. A  $100 \text{ k}\Omega$  load was used.

conflict with its very good S11. It is likely that the RF diodes used are not efficient for rectification at this high frequency, and this may account for much of the reduction in efficiency seen in the fifth band.

### *2.5.3 Multi-excitation response*

An experiment was then performed to characterize the multi-band excitation response of the 2-band prototype. The goal of this experiment is to quantify how well the harvester can combine power from multiple bands.

The multi-excitation experiment consists of a two-band excitation produced by combining the output of two RF function generators. This is a highly controllable cabled experiment which can help quantify the effect of multiple excitations on performance, and quantify the effectiveness of the power combination method used. Only the 2-band prototype was subjected to this experiment. Figure 2.10 illustrates the performance of power combination between bands. Interestingly, the RF-DC conversion efficiency of the entire system increases as more bands are excited.

### *2.5.4 In the wild*

The 5-band harvester was subjected to two scenarios in which “wild” RF energy was present. In the first scenario, it was placed in the field of a UHF RFID reader emitting 30 dBm at 915 MHz into a 6 dBic circularly polarized antenna. At a distance of 5 m from the RFID reader, the harvester was able to produce 2.3 V across a  $100\text{ k}\Omega$  load, for a delivered power of  $53\text{ }\mu\text{W}$ .

In the second scenario, the 5-band harvester was placed at a location 4.2 km distant from a TV broadcast tower emitting 1 MW at 539 MHz, and was able to produce 2.5 V across the same  $100\text{ k}\Omega$  load for a delivered power of  $62.5\text{ }\mu\text{W}$ . These “wild” scenarios appear to indicate that the antenna-connected harvester appears to work serviceably with single-band excitation from two very different RF sources.



Figure 2.11: The 5-band harvester prototype connected to a log-periodic antenna spanning 400-900 MHz.

## 2.6 Conclusions on Multiband Harvesting

The multiband harvester presented in this chapter provides three distinct benefits: (1) RF source flexibility (2) access to additional power and (3) improved sensitivity. RF source flexibility means that the harvester is able to operate using any subset of several potential source frequencies. The second benefit of multiband harvesting is that it provides access to additional power because the harvester can collect energy from multiple RF sources simultaneously. The third benefit is that multiband harvesting can provide improved sensitivity in circumstances in which no one source provides enough power to operate the device, but several sources in combination do.

RF source flexibility is significant because it enables mobile RF harvesting: the frequency of the strongest RF source is not generally the same in each city; the multiband harvester presented here allows a device to capture power from the strongest sources it encounters. The novel diode summation network presented here is crucial for RF source flexibility. A multiband harvester without our diode summation network would require simultaneous excitation in all or most of its input bands. While such a harvester might provide benefits 2 and 3 (increased total power and increased sensitivity), it would not provide benefit 1. One can imagine providing benefit 1 with an actively tunable harvester design, but the active circuitry would typically cost substantial power, resulting in a system with low net efficiency.

In summary, the efficient multiband harvesting presented here can enable mobile RF harvesting, increasing the practicality of ambient RF as a power source.

## Chapter 3

### **NARROWBAND AMBIENT BACKSCATTER**

In order to apply an ambient RF harvesting solution in practical use cases, the power consumption of the connected device must be brought down to match the budget provided by the ambient RF harvester. Since the most power-consuming portion of most connected devices is the communication subsystem, this is the logical subsystem on which to focus when reducing power.

This chapter focuses on a method of using the same ambient signal which provides power to the connected device as a medium for performing communication. This chapter will explain the method of ambient backscatter, the benefits of ambient backscatter over conventional radio in an RF-powered system, and optimizations on ambient backscatter which leverage unique properties of this novel communication technique.

#### ***3.1 Backscatter background***

In 1948, engineer Harry Stockman published an article in the Proceedings of the IRE titled “Communications by means of reflected power.” This paper, which described Stockman’s experiments with rotating retroreflectors, inspired a new communication paradigm in which energy is beamed at a distant target which then reflects (scatters) that energy in such a way as to convey information to a listener stationed at the beams source.[46]

During World War II, allied aircraft had already made use of modulated reflectors to indicate to beam-wielding stations on the ground that they were friendly. After Stockmans 1948 paper, during years of tension between the US and the USSR, an acoustically-modulated scattering device smuggled into the office of the US ambassador to Moscow allowed the Soviets to listen to the ambassadors conversations. This passive listening bug was undiscovered

for seven years.

With the advent of integrated circuits, a new incarnation of this modulated backscatter topology was born in which an interrogator (reader) beams energy at a transponder (tag) which then signals its unique identification number by electrically modulating the scattering coefficient of its antenna, presenting a time-varying radar cross section to the interrogator.

While these methods inspired by Stockman’s 1948 work have proven to be highly impactful, there is still yet unexplored territory tangential to Stockman’s work. While Stockman and all follow-up work focuses on a topology in which energy is intentionally beamed at a transponder and then the modulated signal read back at the location of that beam source, it does not consider the case where the illuminating energy source is unintentional, a part of another communication system which incidentally happens to be nearby.

This case, which will be the focus of this work, is interesting in the context of the modern built environment, which is pervaded by a wash of broad spectrum ambient signaling.

### **3.2 Design of an ambient backscatter system**

The design of our ambient backscatter node avoids the expensive process of generating radio waves; backscatter communication is orders of magnitude more power-efficient than traditional radio communication. Further, since it leverages the ambient RF signals that are already around us, it does not require a dedicated power infrastructure as in conventional backscatter communication (e.g., RFID).

Ambient backscatter differs from RFID-style backscatter in three key respects. Firstly, it takes advantage of existing RF signals so it does not require the deployment of a special-purpose power infrastructure—like an RFID reader—to transmit a high-power (1W) signal to nearby devices. This avoids installation and maintenance costs that may make such a system impractical, especially if the environment is outdoors or spans a large area. Second, and related, it has a very small environmental footprint because no additional energy is consumed beyond that which is already in the air. Finally, ambient backscatter provides device-to-device communication. This is unlike traditional RFID systems in which tags

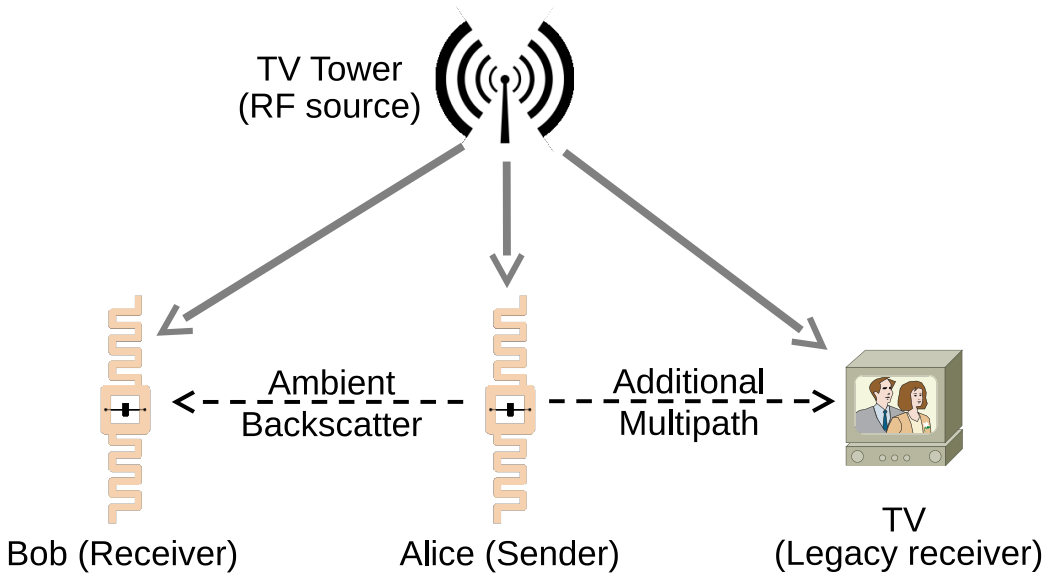


**Figure 3.1: Ambient Backscatter:** Communication between two battery-free devices. One such device, Alice, can backscatter ambient signals that can be decoded by other ambient backscatter devices. To legacy receivers, this signal is simply an additional source of multipath, and they can still decode the original transmission.

must talk exclusively to an RFID reader and are unable to even sense the transmissions of other nearby tags. Figure 3.1 illustrates the core concept of performing ambient backscatter.

To understand ambient backscatter in more detail, consider two nearby battery-free devices, Alice and Bob, and a TV tower in a metropolitan area as the ambient source, as shown in Fig. 3.1. Suppose Alice wants to send a packet to Bob. To do so, Alice backscat-

ters the ambient signals to convey the bits in the packet—she can indicate either a ‘0’ or a ‘1’ bit by switching her antenna between reflecting and non-reflecting states. The signals that are reflected by Alice effectively create an additional path from the TV tower to Bob and other nearby receivers. Wideband receivers for TV and cellular applications are designed to compensate for multi-path wireless channels, and can potentially account for the additional path. Bob, on the other hand, can sense the signal changes caused by the backscattering, and decode Alice’s packet.

Designing an ambient backscatter system is challenging for at least three reasons.

- Since backscattered signals are weak, traditional backscatter uses a constant signal [29] to facilitate the detection of small level changes. Ambient backscatter uses uncontrollable RF signals that already have information encoded in them. Hence it requires a different mechanism to extract the backscattered information.
- Traditional backscatter receivers rely on power-hungry components such as oscillators and ADCs and decode the signal with relatively complex digital signal processing techniques. These techniques are not practical for use in a battery-free receiver.
- Ambient backscatter lacks a centralized controller such as an RFID reader to coordinate all communications. Thus, it must operate a distributed multiple access protocol and develop functionalities like carrier sense that are not available in traditional backscattering devices.

Our approach is to co-design the hardware elements for ambient backscatter along with the layers in the network stack that make use of it. The key insight we use to decode transmissions is that there is a large difference in the information transfer rates of the ambient RF signal and backscattered signal. This difference allows for the separation of these signals using only low-power analog operations that correspond to readily available components like capacitors and comparators. We are similarly able to realize carrier sense and framing operations with low-power components based on the physical properties of ambient backscatter

signals. This in turn lets us synthesize network protocols for coordinating multiple such devices.

The following sections detail the design of the ambient backscatter transmitter and receiver, respectively.

### *3.2.1 Design of an ambient backscatter transmitter*

The design of our ambient backscattering transmitter builds on conventional backscatter communication techniques. At a high level, backscattering is achieved by changing the impedance of an antenna in the presence of an incident signal. Intuitively, when a wave encounters a boundary between two media that have different impedances/densities, the wave is reflected back [26]. The amount of reflection is typically determined by the difference in the impedance/density values. This holds whether the wave is a mechanical wave that travels through a rope fixed to a point on a wall or an electromagnetic wave encountering an antenna. By modulating the electrical impedance at the port of the antenna one can modulate the amount of incident RF energy that is scattered, hence enabling information to be transmitted.

To achieve this, the backscatter transmitter includes a switch that modulates the impedance of the antenna and causes a change in the amount of energy reflected by the antenna. The switch consists of a transistor connected across the two branches of the dipole antenna. The input signal of the switch is a sequence of one and zero bits. When the input is zero, the transistor is off and the impedances are matched, with very little of the signal reflected. When the switch input signal is one, the transistor is in a conducting stage which shorts the two branches of the antenna and results in a larger scattered signal amplitude. Thus, the switch toggles between the backscatter (reflective) and non-backscatter (absorptive) states to convey bits to the receiver.

We note the following about our design: Firstly, the communication efficiency is high when the antenna topology is optimized for the frequency of the ambient signals. Our implementation uses a 258 millimeter dipole antenna, optimized for a 50 MHz subset (in this

case, from 515-565 MHz) of the UHF TV band. Other antenna topologies such as meandered antennas [39] and folded dipoles [38] can result in smaller dimensions, and further design choices can be made to increase the bandwidth of the antenna in order to make it capable of utilizing a larger frequency band. However, exploring this design space is not within the scope of this paper.

Secondly, RF switches can have a large difference between their conducting and non-conducting impedance values, but only in the specific frequency range that they are designed for. For example, using a switch that is optimized for use in RFID tags that operate in 915 MHz would not be optimal for ambient backscatter of lower-frequency TV signals. Thus, the ambient backscattering transmitter should select a switch that is optimal for the operational frequencies of the ambient signals.

Finally, the switches and antennas are not designed to specifically backscatter and receive on a particular TV channel. For example, in ATSC, each TV channel has a 6 MHz bandwidth and different TV channels are typically allocated to adjacent non-overlapping frequencies. Since ambient backscattering devices backscatter all these signals, they do not require fine tuning for each frequency and can work as long as there are TV transmissions on at least one of the frequencies.

### *3.2.2 Ambient Backscattering Receiver*

Designing an ambient backscatter receiver is challenging for two main reasons: First, ambient signals already encode information and hence backscattering additional information over these signals can be difficult. Second, the backscattered information should be decodable on an ultra-low-power device without using power-hungry hardware components such as ADCs and oscillators. To address these challenges, we first show how one can extract the backscattered information from the ambient signals using a conventional digital receiver. We then describe an ultra-low-power receiver design that uses only analog components.

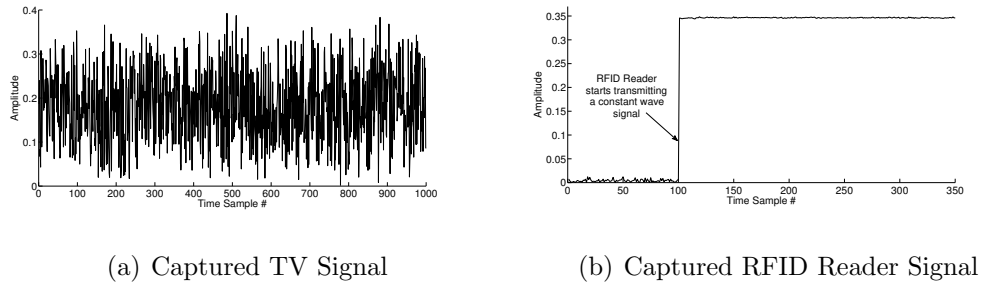


Figure 3.2: Comparison of the incident signal on a backscattering transmitter's antenna in both (a), ambient backscatter, and (b), conventional RFID.

# *Extracting Backscatter Information from Ambient Signals*

Ambient signals like TV and cellular transmissions encode information and hence are not controllable. To illustrate this, Fig. 3.2(a) shows an example of the time-domain ambient TV signal captured on a USRP operating at 539 MHz. For comparison, Fig. 3.2(b) plots the typical time domain signal received on a USRP from an RFID reader transmitting at 915 MHz. While the traditional RFID transmission is a constant amplitude signal, the ambient TV signal varies significantly in its instantaneous power. This is expected because the captured ATSC TV signals encode information using 8VSB modulation, which changes the instantaneous power of the transmitted signal. Thus, the receiver should be capable of decoding the backscattered signals in the presence of these fast changing signals.

In this section, we describe our mechanism assuming a powerful digital receiver that samples the analog signal and performs demodulation and decoding in the digital domain. In the next section, we extend it to work using only analog components.

Our key insight is that if the transmitter backscatters information at a lower rate than the ambient signals, then one can design a receiver that can separate the two signals by leveraging the difference in communication rates. Specifically, ambient TV signals encode information at a bandwidth of 6 MHz, so if we ensure that the transmitter backscatters information at

a larger time-scale than 6 MHz, then the receiver can extract the backscattered information using averaging mechanisms. Intuitively, this works because the wideband ambient TV signals change at a fast rate and hence adjacent samples in TV signals tend to be more uncorrelated than the adjacent samples in the backscattered signals. Thus, averaging the received signal across multiple samples effectively removes the variations in the wideband ambient TV signals, allowing the backscattered signals to be decoded.

For completeness, we formally describe why this works. Say we have a digital receiver that samples the received signal at the Nyquist-information rate of the TV signal. The received samples,  $y[n]$ , can then be expressed as a combination of the wideband TV signals and the backscattered signals, i.e.,

$$y[n] = x[n] + \alpha B[n]x[n] + w[n]$$

where  $x[n]$ s are the samples corresponding to the TV signal as received by the receiver,  $w[n]$  is the noise,  $\alpha$  is the complex attenuation of the backscattered signals relative to the TV signals, and  $B[n]$  are the bits transmitted by the backscattering transmitter. Since the receiver samples at the TV Nyquist rate, the adjacent samples in  $x[n]$  are uncorrelated. Now, if the backscatterer conveys information at a fraction of the rate, say  $\frac{1}{N}$ , then  $B[Ni+j]$ s are all equal for  $j = 1$  to  $N$ .

If the receiver averages the instantaneous power in the  $N$  receiver samples corresponding to a single backscattered bit, then we get:

$$\frac{1}{N} \sum_{i=1}^N |y[n]|^2 = \frac{1}{N} \sum_{i=1}^N |x[n] + \alpha Bx[n] + w[n]|^2$$

where  $B$  is either ‘0’ or ‘1’. Since the TV signal,  $x[n]$ , is uncorrelated with noise,  $w[n]$ , we can rewrite the above equation as:

$$\frac{1}{N} \sum_{i=1}^N |y[n]|^2 = \frac{|1 + \alpha B|^2}{N} \sum_{i=1}^N |x[n]|^2 + \frac{1}{N} \sum_{i=1}^N w[n]^2$$

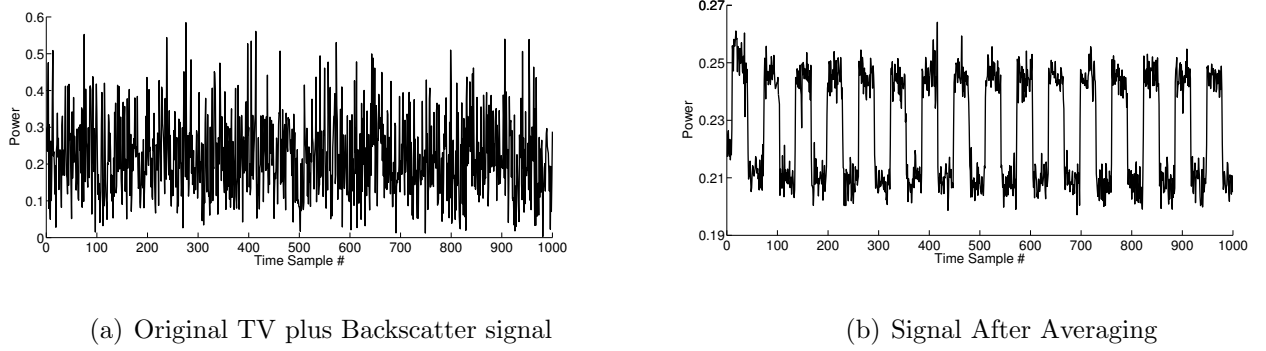
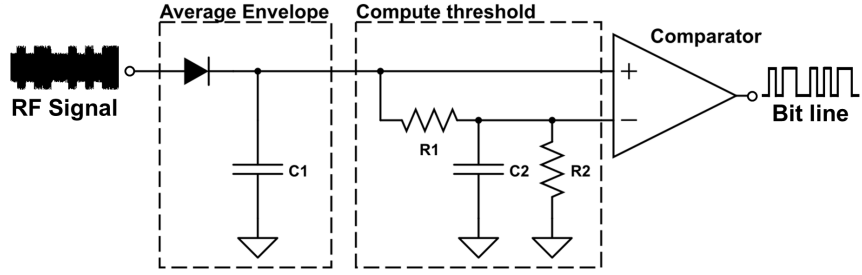


Figure 3.3: Comparison of backscattered signal received both with (b) and without (a) averaging.

Say  $P$  is the average power in the received TV signal, i.e.,  $P = \frac{1}{N} \sum_{i=1}^N |x[n]|^2$ . Ignoring noise, the average power at the receiver is  $|1 + \alpha|^2 P$  and  $P$  when the transmitter is in the reflecting and non-reflecting states, respectively. The receiver can distinguish between the two power levels,  $|1 + \alpha|^2 P$  and  $P$ , to decode the information from the backscattering transmitter. Thus, even in the presence of changes in the TV signal, the receiver can decode information from the backscattering transmitter.

We apply the above mechanism to the ambient ATSC TV signals [1]. Specifically, we set our ambient backscattering transmitter to transmit an alternating sequence of ones and zeros at a rate of 1kbps. Fig. 3.3(a) plots the received signal on an USRP that is placed one foot from the transmitter. Fig. 3.3(b) plots the effect of averaging every 100 received samples. As the figure shows, averaging reduces the effect of the fast-varying ambient TV signals. Further, the receiver can now see two average power levels which it can use to decode the backscattered information.

We note that ambient backscatter can either increase or decrease the average power of the received signal. Specifically, the channel,  $\alpha$ , is a complex number and hence  $|1 + \alpha|$  can be either less than or greater than one. This means that a zero bit can be either a lower power than the average power,  $P$ , in the TV signal, or can have a higher power than the



**Figure 3.4: Circuit Diagram for the Demodulator:** The demodulator has two stages: an envelope detection and averaging stage that produces an average envelope of the signal, and a compute-threshold stage that compares the averaged signal with a threshold value computed by taking a longer-term average of the signal.

average. Intuitively, this is because the additional multi-path created by the backscattering transmitter can either constructively or destructively interfere up with the existing signal. We use differential coding to eliminate the need to know the extra mapping between the power levels and the bits (see 3.3.1).

#### *Decoding on an Ultra-Low-Power Device*

The above design assumes that the receiver can get digital samples on which it can perform operations like averaging and comparison of power levels. However, acquiring digital samples requires an analog-to-digital converter (ADC) which can consume a significant amount of power and is typically avoided in ultra-low-power designs [49]. In this section, we imitate the above operations in analog hardware by selecting an appropriate analog circuit topology.

As shown in Fig. 3.4, our receiver has two stages: an envelope detection and averaging circuit that smoothens out the natural variations in the TV signal, and a compute-threshold circuit that produces a threshold between the two levels. A comparator compares the average envelope signal to the threshold to generate output bits.

**Average Envelope stage:** This circuit is implemented using an envelope detector and RC

(resistive/capacitive) circuit to smooth/average out the natural variations in the TV signals. As shown in Fig. 3.4, it has two simple hardware elements: a diode and a capacitor  $C_1$ , and also makes use of a current path through two serial resistors,  $R_1$  and  $R_2$ . To a first approximation, diodes act as one-way valves, allowing current to flow in one direction but not the other, capacitors are charge storage elements, and resistors regulate current flow. In this circuit, the diode provides charge whenever the input voltage is greater than the voltage at the capacitor. During the time period when the input is lower than the voltage on the capacitor, the diode does not provide charge and the resistors slowly dissipate the energy stored on the capacitor, lowering the voltage. The rate of drop of voltage is roughly determined by the product  $C_1(R_1 + R_2)$ . Thus, by balancing the values of  $R_1$  and  $R_2$  against the effective resistance of the diode and selecting an appropriate capacitance, the circuit shown can act as a low-pass filter, averaging out the fast natural variations in the TV signals but preserving the slowly varying backscattered bits.

**Compute-Threshold stage:** The output of the averaging circuit produces two signal levels, corresponding to the ‘0’ and the ‘1’ bits. In principle, a receiver with an ADC can distinguish between the two signal levels by processing the digital samples. Specifically, say we have two signals with different voltages,  $V_0$  and  $V_1$ ,  $V_1 > V_0$ , where  $V_0$  and  $V_1$  correspond to the power levels for the zero and one bits. To distinguish between them, the receiver would first compute a threshold value which is the average of the two signal levels, i.e.,  $\frac{V_0+V_1}{2}$ . When the received signal is greater than this threshold, we conclude that the received signal is  $V_1$ ; otherwise, we conclude that the received signal is  $V_0$ .

Since we choose to eliminate the need for a full ADC in order to reduce power, the receiver imitates this operation using analog hardware. Fig. 3.4 shows the hardware elements used by the comparison circuit. It consists of an RC circuit and a comparator. The RC circuit re-uses the two resistors ( $R_1$  and  $R_2$ ) and adds a capacitor ( $C_2$ ) to perform further averaging, producing a threshold value of near  $\frac{V_0+V_1}{2}$ . The comparator takes two voltage values as inputs and produces either a one or a zero to indicate which of the two values is larger. The first input to the comparator is the output of our average envelope circuit and the second input

is the threshold value.

We note that the bit rate of the prototype dictates the choice of values for the RC circuit elements (e.g., a receiver operating at 10 kbps requires different RC values than one at 1 kbps). This is because, at lower rates, each bit occupies more time on the channel and hence requires more averaging to correctly compute the threshold value. 3.4 describes the parameters used in our implementation.

Finally, while in theory we can distinguish between any two power levels by sufficient averaging, each comparator comes with a minimum gap below which it cannot distinguish between the two power levels. This gap determines the maximum distance at which two devices can communicate with each other.

### **3.3 Network Stack Design**

The network stack design for ambient backscatter communication is closely integrated with the properties of the circuits and the hardware described so far. In this section, we explore the physical layer and the link layer design for ambient backscatter.

#### *3.3.1 Physical Layer*

The physical layer for ambient backscatter communication addresses questions such as what modulation and coding to use, how to perform packet detection, and how to find bit boundaries.

*Modulation and Bit Encoding:* Since a backscattering transmitter works by switching between reflecting and non-reflecting states, it effectively creates an ON-OFF keying modulation. However, as described earlier, the backscattered signal could either constructively or destructively interfere with the ambient TV signal. Thus, depending on the receiver’s location, a ‘1’ bit could appear as either an increase or a decrease in the received power. To address this issue, the physical layer uses FM0 coding [25]. FM0 coding turns every bit into two symbols and encodes information using symbol transitions [25]. FM0 has a symbol

transition at the beginning of every bit period along with an additional mid-bit transition to represent a ‘1’, and no such transition in the ‘0’ bit. Thus, bits are encoded using transitions in the power level, rather than the actual power levels; further, it guarantees an equal number of ‘0’ and ‘1’ symbols.

*Detecting the Beginning of a Packet Transmission:* At the beginning of each packet transmission, an ambient backscattering transmitter sends a known preamble that the receiver detects using bit-level correlation on the digital hardware (in our case, the microcontroller). However, unlike RFID communication, where the tags correlate only when they are powered by a nearby reader, an ambient backscatter device does not know when nearby devices will transmit and hence might have to continuously correlate, which is power-consuming and impractical for a low-power device.

We avoid continuous correlation by only activating the relatively expensive correlation process when the comparator detects bit transitions. The comparator hardware takes very little power and has a built-in threshold before it detects bit transitions (in our implementation, this threshold is 2.4 mV). It is only when the power difference crosses this threshold that an interrupt is sent to the digital hardware to wake it up from its idle state (to perform correlation). Since the averaging circuit eliminates the large variations in the ambient TV signal, it is unlikely that ambient signals alone create changes in the power level in the absence of a packet transmission.

To provide the hardware with sufficient leeway to wake up the digital hardware, as shown in Fig. 3.5, the transmitter sends a longer preamble that starts with an alternating 0-1 bit sequence before sending the actual preamble. The alternating bit sequence is long enough (8 bits in our implementation) to wake up the digital hardware, which then uses traditional mechanisms to detect bit boundaries and perform framing.

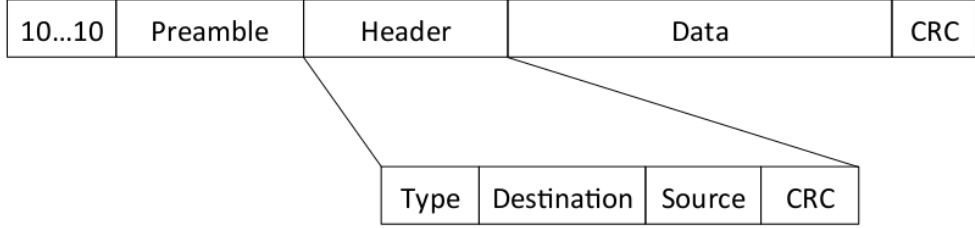


**Figure 3.5: Packet Format:** Each packet starts with an alternating sequence of ‘1’s and ‘0’s followed by a preamble that is used by the receiver to detect packets. The preamble is followed by a header and then the data, which both include CRCs used to detect bit errors.

### 3.3.2 Link Layer

## 3.4 A prototype ambient backscatter communicator

To show the feasibility of our ideas, we have built a hardware prototype, shown in Fig. 3.6, that is approximately the size of a credit card.<sup>1</sup> Our prototype includes a power harvester for TV signals, as well as the ambient backscatter hardware that is tuned to communicate by using UHF TV signals in a 50 MHz wide frequency band centered at 539 MHz. The harvested energy is used to provide the small amounts of power required for ambient backscatter and to run the microcontroller and the on-board sensors. Our prototype also includes a low-power flashing LED and capacitive touch sensor for use by applications.

We implement our prototype on a 4-layer printed circuit board (PCB) using off-the-shelf circuit components. The PCB was designed using Altium design software and was manufactured by Sunstone Circuits. A total of 20 boards were ordered at a cost of \$900. The circuit components were hand-soldered on the PCBs and individually tested which required a total of 50 man-hours. As shown in Fig. 3.6, the prototype uses a dipole antenna that consists of two 2 sections of 5.08 in long 16 AWG magnetic copper wire. The prototype’s

---

<sup>1</sup>We use off-the-shelf components to design and build our prototype. A production integrated circuit would achieve better results and be of an arbitrary form factor (down to  $1 \text{ mm}^2$  plus the antenna).

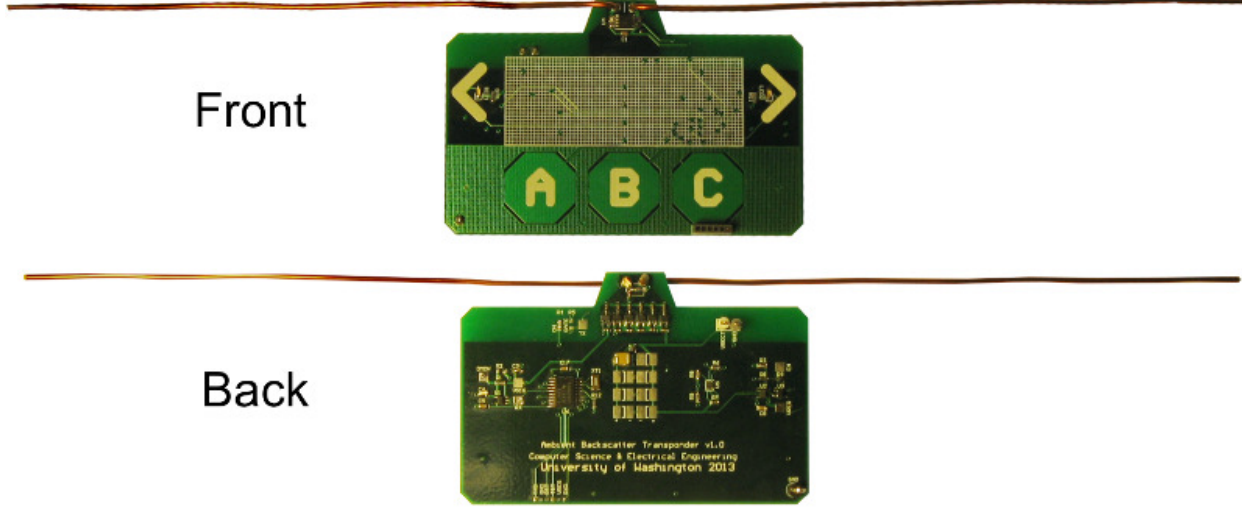


Figure 3.6: **Prototype:** A photo of our prototype PCB that can harvest, transmit and receive without needing a battery or powered reader. It also includes touch sensors (the A, B and C buttons), and LEDs (placed near the two arrows) that operate using harvested energy and can be programmed by an onboard microcontroller.

harvesting and communication components are tuned to use UHF TV signals in the 50 MHz band centered at 539 MHz<sup>2</sup>.

The transmitter is implemented using the ADG902 RF switch [3] connected directly to the antenna. The packets sent by the transmitter follow the format shown in Fig. 3.5. Further, it is capable of transmitting packets at three different rates: 100 bps, 1 kbps, and 10 kbps. We also implement both preamble correlation and energy detection in digital logic to perform carrier sense at the transmitter. Our implementation currently does not use error correction codes and has a fixed 96-bit data payload with a 64-bit preamble.

Our implementation of the receiver circuit, described in 3.2.2, uses TS881 [6], which is an ultra-low-power comparator. The output of the comparator is fed to the MSP430

---

<sup>2</sup>To target a wider range of frequencies, one can imagine using a frequency-agile, auto-tuning harvester that autonomously selects locally available channels, with a design similar to the dual-band RFID tag in [44].

Table 3.1: **Power Consumption of Analog Components**

	Tx	Rx
Ambient Backscatter	$0.25\mu W$	$0.54\mu W$
Traditional Backscatter (WISP [43])	$2.32\mu W$	$18\mu W$

microcontroller which performs preamble correlation, decodes the header/data and verifies the validity of the packet using CRC. We implement different bit rates by setting the capacitor and resistor values,  $R_1$ ,  $R_2$ ,  $C_1$ , and  $C_2$  in Fig. 3.4, to  $(150 \text{ } k\Omega, 10 \text{ } M\Omega, 27 \text{ } nF, 200 \text{ } nF)$  for 100 bps,  $(150 \text{ } k\Omega, 10 \text{ } M\Omega, 4.7 \text{ } nF, 10 \text{ } nF)$  for 1 kbps, and  $(150 \text{ } k\Omega, 10 \text{ } M\Omega, 680 \text{ } pF, 1 \text{ } \mu F)$  for 10 kbps.

Table 3.1 compares the power consumption of the analog portion of our transmitter/receiver with that of the WISP, an RFID-based platform[43]. The table shows that the power consumption numbers for ambient backscatter are better than the WISP platform, and almost negligible given the power budget of our device. This is because ambient backscatter operates at lower rates (10 kbps) when compared to existing backscatter systems like the WISP, which operates at 640 kbps. So, we were able to optimize the power consumption of our prototype and achieve lower power consumption values.

Our prototype also includes two sensing and I/O capabilities for our proof-of-concept applications that are controlled by the microcontroller: low-power flashing LEDs and capacitive touch buttons implemented on the PCB using a copper layer. However, these sensors as well as the microcontroller that drives them can significantly add to the power drain. In fact, in a smart card demonstration application, the transmit modulator consumed less than 1% of the total system power, while the demodulator required another 1%; demonstrating that ambient backscatter significantly reduces the communication power consumption. The power management circuitry required an additional 8% of the total power. Flashing the LEDs and polling the touch sensors at the intervals used in consumed 26% of the total

power. The remaining 64% was consumed by the microcontroller.<sup>3</sup>

We note that in scenarios where the TV signal strength is weak, our prototype uses duty cycling to power the sensors and the microcontroller. Specifically, when the prototype is in the sleep mode, it only harvests RF signals and stores it on a storage capacitor. Once enough energy has been accumulated on the capacitor, it goes into active mode and performs the required operations. In hardware, the duty cycle is implemented by a voltage supervisor that outputs a high digital value (indicating active mode) when the voltage on the storage capacitor is greater than 1.8 V.

### ***3.5 Improving rate and range of ambient backscatter***

Wi-Fi systems today can achieve bit rates as high as 300 Mbps [7] and cellular networks can operate at ranges of tens of kilometers [8]. These impressive rate and range capabilities have been made possible by communication primitives such as coding mechanisms and multi-antenna processing. These techniques, however, are not suitable for battery-free devices such as RFID tags and ambient power harvesting sensors: Existing multi-antenna designs consume power on the order of a few Watts [16]; this is orders of magnitude more power than is available on harvesting devices [24]. Similarly, coding techniques that enhance communication range and enable concurrent transmissions (e.g., CDMA) consume substantial power and computational resources that limit their applicability to low-power devices.

The key reason for this is that these techniques assume the ability to perform complex digital signal processing — multi-antenna processing requires estimating channel parameters and performing operations such as matrix inversion; coding techniques (e.g., CDMA) require performing computationally expensive correlation and synchronization. These methods are infeasible on battery-free devices as obtaining a digital representation of a signal requires

---

<sup>3</sup>We note that the high power consumption for the digital circuit (i.e., microcontroller) is an artifact of our prototype implementation. Specifically, the microcontroller is a general-purpose device that is not typically used in commercial ultra-low-power devices. Instead, commercial systems use Application-Specific Integrated Circuits (ASICs) that can consume orders of magnitude less power than general-purpose solutions [35, 43]. In ASIC-based low-power devices, the power consumption of the analog components often dominates that of the digital circuit [10].

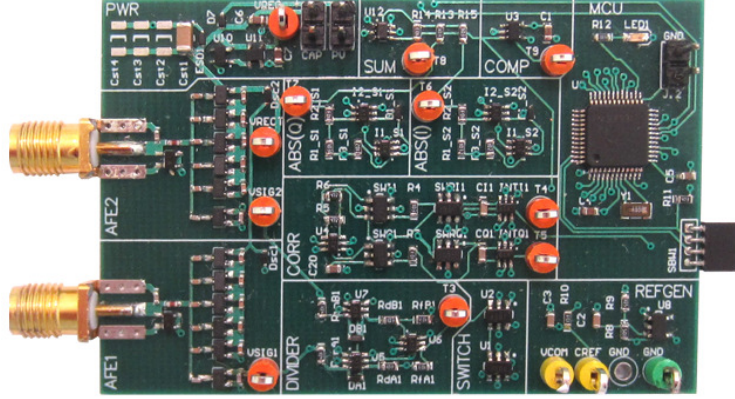


Figure 3.7: A prototype of the “turbocharged” ambient backscatter system, which integrates both  $\mu\text{mo}$  and  $\mu\text{code}$  in a single design. It can operate using both RFID and TV transmissions[32].

power-intensive ADCs, and performing computationally expensive tasks is also expensive in terms of power consumption.

In this work, we ask if it is possible to achieve the benefits of these communication primitives on RF-powered devices. The intuition we leverage is as follows: since the power-intensive nature of these techniques is due to their use of ADCs and digital computation, if we instead perform computation in the analog domain we can achieve orders of magnitude reduction in the power consumption. Using this as our guiding principle, we design two communication primitives for backscatter communication:  $\mu\text{mo}$ , a multi-antenna receiver that is powered using harvested energy, and  $\mu\text{code}$ , a low-power coding mechanism that enables large communication ranges and concurrent transmissions, and can be decoded using simple analog components on battery-free devices[32].

### 3.5.1 Leveraging system properties with $\mu\text{MO}$

We present a multi-antenna technique that enables Alice’s receiver to decode Bob’s backscattered transmission without estimating the channel parameters. The intuition underlying our

approach is best explained using an example. Let  $s(t)$  be the signal from the TV tower and suppose Bob conveys ‘1’ (‘0’) bit by reflecting (not reflecting) the TV signals. Alice now receives the following signals on its two antennas:

$$\begin{aligned}y_1(t) &= h_{rf}s(t) + h_bBs(t) \\y_2(t) &= h'_{rf}s(t) + h'_bBs(t)\end{aligned}$$

where  $h_{rf}, h'_{rf}$  and  $h_b, h'_b$  are the channels from the TV tower and Bob to the two antennas on Alice, respectively. Further,  $B$  is 1 when Bob reflects the signals and is 0 otherwise.

$\mu$ mo decodes the backscattered bits without estimating any channel parameters. Specifically, the receiver computes  $\frac{y_1(t)}{y_2(t)}$  which is either  $\frac{h_{rf}}{h'_{rf}}$  or  $\frac{h_{rf}+h_b}{h'_{rf}+h'_b}$  depending on whether the backscattered bit is ‘0’ or ‘1’. Thus, the receiver can decode the backscattered data without performing channel estimation. We explore the above idea further and describe how the above operation can be performed using simple analog components, without requiring digital computation.

### 3.5.2 Applying coding with $\mu$ Code

Coding mechanisms such as CDMA can in principle be used to increase the communication range of backscatter systems. These techniques use a string of pseudorandom bits called chips to encode information bits. For example, the transmitter could represent a zero bit by the chip sequence ‘101110111’ and a one bit by the chip sequence ‘111011011’. The 1s and 0s in the above sequences are the chips used by the transmitter to encode the information. To decode these information bits, the receiver correlates the received signal with the chip sequence patterns and converts correlation peaks to data bits. To increase the communication range, the transmitter-receiver pair uses longer chip sequences that effectively increase the signal-to-noise ratio and hence enable long-range communication. Decoding such transmissions on a backscatter device is challenging for two main reasons:

- The correlation operation required at the receiver is both computationally expensive and requires power-consuming ADCs that are not available on a backscatter device.

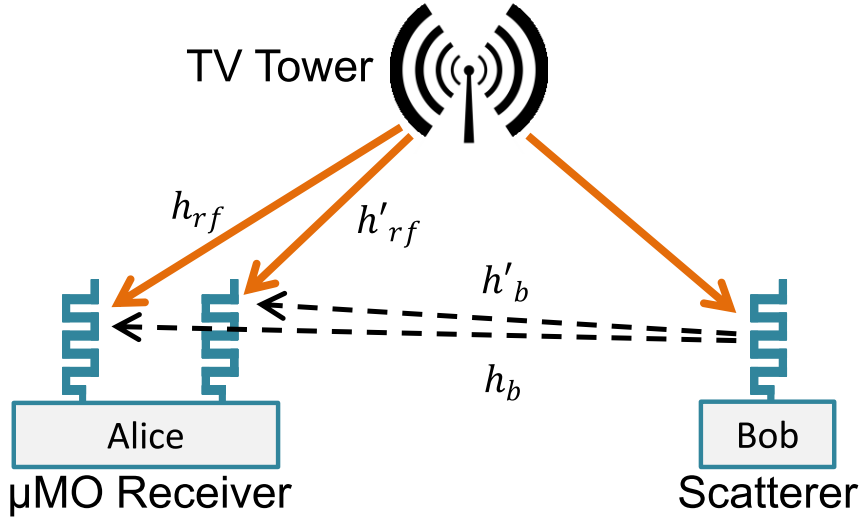


Figure 3.8:  **$\mu$ mo Decoding.** The two-antenna device, Alice, can decode Bob’s backscattered information by separating the direct TV transmissions from the backscattered signals.  $\mu$ mo achieves this operation with neither channel estimation nor digital computation.

- More important, performing synchronization at the receiver is expensive. Synchronization requires correlating the received signal with a chip sequence for every offset of the received signal. This is not only computationally expensive but also consumes much more power than is available on our target device.

So any code that is to be decoded on a backscatter device should satisfy two main properties: 1) It should not require an ADC or digital signal processing operations, and 2) It should work without the need for synchronization.

$\mu$ code can achieve coding gains on the backscatter device without requiring synchronization operations at the receiver. To understand  $\mu$ code, we first explain the intuition using a simple sinusoidal wave; we then design the encoding and decoding algorithms to operate on the backscattered bits.

Intuitively, instead of using a pseudorandom chip sequence,  $\mu$ code uses a periodic signal to represent the information. To see why this works, consider a periodic sinusoidal signal

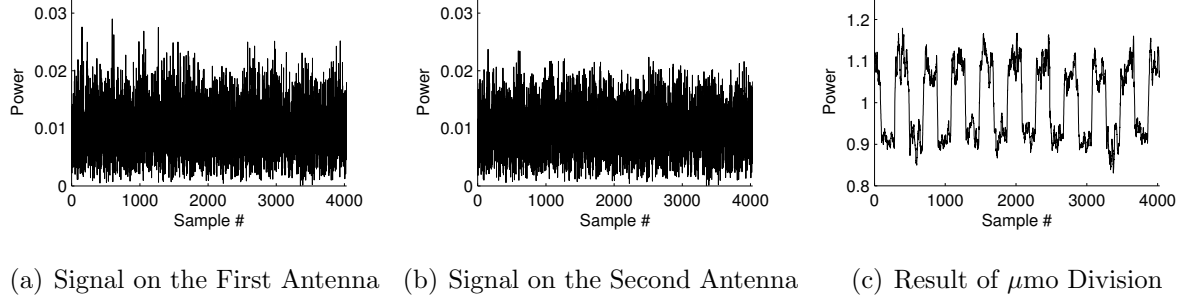


Figure 3.9:  $\mu\text{mo}$  on actual signals. It is difficult to see the backscattered bits on the received signals at the two receiver antennas. Performing the division between the received signals on the two antennas, reveals the backscattered bits[32].

transmitted at a specific frequency. If the receiver knows the frequency of the sinusoidal signal, it can detect the signal without any phase synchronization with the transmitter. Specifically, suppose the transmitter sends a sine wave,  $\sin(ft + \phi)$ , with a frequency  $f$  and a phase offset  $\phi$ . One can easily detect the above sine wave without phase synchronization by performing a dot product operation with the sine and cosine basis functions at the same frequency to compute the In-phase (I) and Quadrature phase (Q) components:

$$I = \sum_{t=0}^T \sin(ft + \phi) \sin(ft) \Delta t = \frac{1}{2} \sin(\phi)$$

$$Q = \sum_{t=0}^T \sin(ft + \phi) \cos(ft) \Delta t = \frac{1}{2} \cos(\phi)$$

where  $T$  is the duration over which the above dot product operation is computed.<sup>4</sup> Note that from the above equation,

$$|I|^2 + |Q|^2 = \frac{1}{2} \quad (3.1)$$

Since Eq. 3.1 is independent of the phase offset  $\phi$  the receiver can detect the transmitted signal without the need for phase synchronization. Further, the receiver can increase its

---

<sup>4</sup>We replace the integration operation that is typically performed with summation, for ease of exposition.

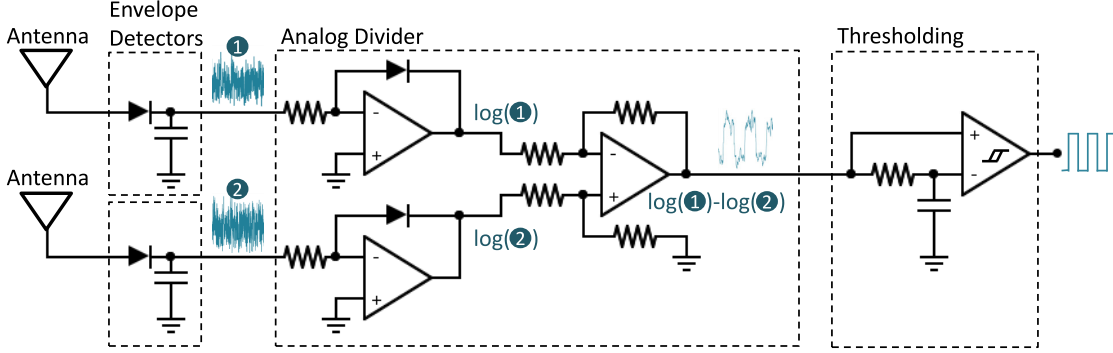


Figure 3.10:  **$\mu$ mo hardware design.**  $\mu$ mo performs the required computation using analog components. Specifically,  $\mu$ mo’s hardware has three main components: an envelope detector that removes the carrier frequency (e.g., 539 MHz), an analog division circuit that divides the received signal on the two antennas, and finally a thresholding circuit that outputs the 0 and 1 bits.

detection sensitivity by increasing the transmit signal duration,  $T$ . Thus, a simple periodic sine wave can be detected without requiring phase synchronization, and also provides a form of coding gain to increase reliability.

$\mu$ code’s design builds on the above intuition. However, since our backscatter transmitter has only two states and therefore cannot transmit sine waves, it instead uses a periodic alternating sequence of zeros and ones. Specifically, it encodes the one bit by the chip sequence  $101010\cdots 10$  and the zero bit by the chip sequence  $000000\cdots 00$ .

Our decoder imitates the I and the Q computation above to detect the alternating one-zero sequence, without the need for synchronization. Specifically, it computes the in-phase component (I) by a dot-product operation with the chip sequence  $101010\cdots 10$  and the quadrature-phase component (Q) by a dot-product operation with a 90 degree offset chip sequence. This is similar to using the sine and the cosine function in the previous scenario. Note that a 90 degree offset is effectively a time offset of half a chip duration. To detect the presence of the alternating sequence of zeros and ones, the receiver then computes  $|I| + |Q|$ .

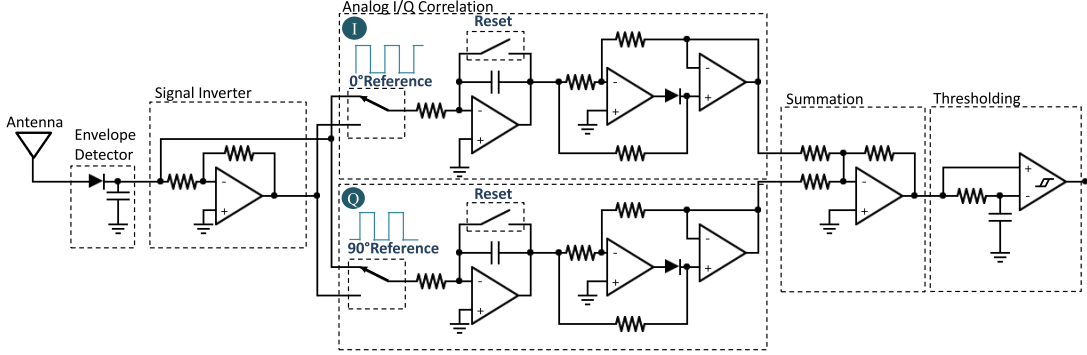


Figure 3.11:  **$\mu$ code hardware design.** Our hardware design performs the decoding operations using analog components, without the need for ADCs. The hardware system has three main components: I/Q correlation circuits that compute  $|I|$  and  $|Q|$ , a summation circuit that computes  $|I| + |Q|$ , and finally a thresholding circuit that outputs 0 and 1 bits.

This works independent of synchronization.

$|I| + |Q|$  is constant, independent of receiver synchronization. Thus the receiver can detect an alternating sequence of zeros and ones by computing  $|I| + |Q|$  over any duration of  $N$  chips. To summarize:

**$\mu$ code's Encoding Algorithm.** The transmitter uses the following chip sequences to represent the zero and one information bits:

$$1010 \dots N \dots 10 \quad \text{as bit 1}$$

$$0000 \dots N \dots 00 \quad \text{as bit 0}$$

where the chips are transmitted at a rate of  $C$ .

**$\mu$ code's Decoding Algorithm.** The receiver computes  $|I| + |Q|$  over a duration of  $\frac{n}{3}$  chips. If the majority vote of three adjacent computations is greater than a threshold then the receiver outputs a 1, and a 0 otherwise. The threshold is computed by taking the average of the received signal over bits in the preamble at the beginning of the transmitted packet.

The transmitter can control both the chip rate  $C$  and the chip length  $N$  to achieve different bit rates. The chip rate determines the duration of each chip bit; a higher chip rate corresponds to smaller chip durations. Given a chip rate, longer chip lengths result in larger ranges since they increase the signal-to-noise ratio. We also showed that by controlling these parameters, we can create orthogonal codes that do not require any synchronization and can enable multiple concurrent transmissions.

## Chapter 4

# WIDEBAND AMBIENT BACKSCATTER

The work done thus far in this project towards employing ambient RF in connected devices has resulted in two key innovations: Multiband RF harvesting and ambient backscatter communication. These represent significant progress towards improving the reliability and coverage area of RF energy harvesting power supplies, and towards reducing the power requirements for connectivity on RF harvesting devices.

### **4.1 Challenges and Goals**

The previous chapters introduced techniques for simultaneously harvesting energy and communicating via scattering of ambient radio signals. In these systems, a single ambient source was employed for both scattering and harvesting energy.

Demonstrations of the ambient backscatter system thus far have been limited to carefully positioned prototypes operating mostly in controlled laboratory experiments. This is a far cry from realizing the true potential of ambient backscatter as a tool for near-ubiquitous low-power communication.

Much like the problem plaguing conventional ambient RF harvesters, and which was remedied by the introduction of the multiband harvester described in Chapter 2, single-source ambient backscatter suffers from severe fading issues. A high incident signal power requirement coupled with reliance on a single ambient RF source results in frequent blackout zones, where devices can neither be sufficiently powered nor communicate.

Further, single-band ambient backscatter requires manual tuning and re-tuning to achieve optimal performance across deployment locations (for instance, between cities). Without significant automated tunability, this narrowband strategy will never result in a single system

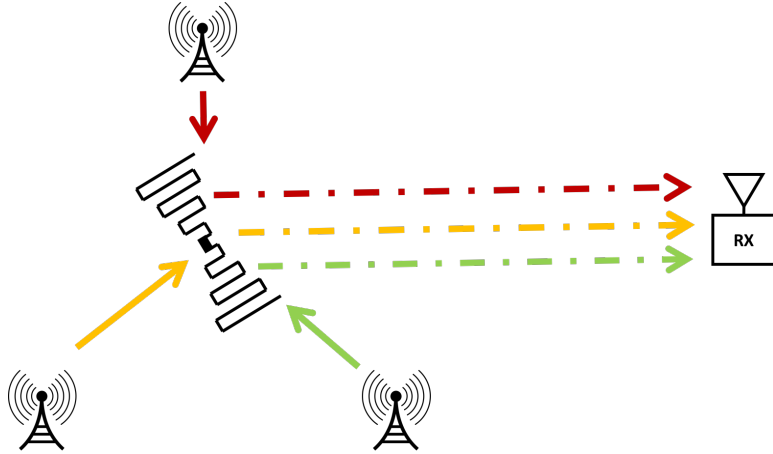


Figure 4.1: To achieve frequency diversity, an ambient backscatter device must be able to re-radiate multiple bands simultaneously. A receiver makes intelligent decisions about which bands to listen for.

capable of operating at any location.

The work presented in this chapter involves connecting some of the dots between multi-band harvesting and ambient backscatter, bringing these communication systems into the realm of more practical applicability.

#### 4.1.1 Making use of all bands

In conventional radios, several methods are used to mitigate fading. Transmit power may be adjusted so that the effect of fading is reduced. Spatial diversity may be applied through the use of multiple antennas. Frequency diversity may be applied, as different operating frequencies produce spatial nulls in different locations.

In ambient backscatter, it is not possible to adjust transmit power, as an upper limit for the re-radiated power is imposed by the power in the impinging signal itself. Further, in many applications it may not be reasonable to expect multiple antennas to be deployed: multiple antennas increase system cost and complexity, and for antennas to have the desired spatial diversity they must be separated by a significant fraction of the carrier wavelength,

something not feasible within the form factor constraints of small embedded sensor nodes.

Because transmit power is not adjustable and attaining spatial diversity is not feasible, this leaves frequency diversity as the obvious option for eliminating operational dead zones. Luckily, there are a plethora of ambient sources available in widely varying frequency bands, with a particular concentration of high-power broadcast transmitters such as television and FM radio signals in the VHF and UHF bands. Non-broadcast sources such as mobile base transceiver stations (cell towers) and also represent significant power sources across the UHF band[27]. Figure 4.1 represents the scenario we are trying to produce.

We explore two methods of achieving frequency diversity by leveraging multiple available ambient signals. First, we briefly introduce a multiband backscatter system and describe the associated challenges. Finally, we introduce and describe in depth a wideband ambient backscatter system which achieves frequency diversity with a simple and practical design, albeit with a different intended use case.

#### *4.1.2 A First Approach*

As in multiband ambient harvesting, if an ambient backscatter system were able to make use of multiple frequencies simultaneously to take advantage of changes in its immediate spectral environment, this would achieve a frequency diversity effect which could improve the range and reliability of ambient backscatter.

One method of implementing this diversity is through multiband ambient backscatter. In this topology, a single wideband antenna is connected to a frequency diplexing network equivalent to that of the multiband ambient RF harvester of Chapter 2. Each band is then routed to an ambient backscatter transceiver identical to that presented in Section 3.2, as well as a rectifier for power recovery. The transceiver I/O signals are connected to a logic controller. Rectifier outputs are combined at DC as in the classic multiband RF harvester of Chapter 2, and used to power the logic controller and transceivers.

To prove the technical feasibility of this concept, the multiband harvester of Chapter 2 was modified as described to allow it to perform tag-to-tag ambient backscatter independently

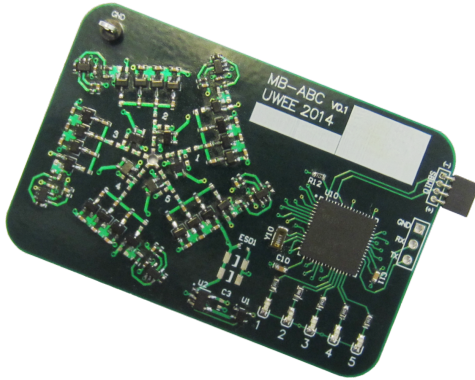


Figure 4.2: A multiband ambient backscatter prototype

across each of five bands, incorporating both independent transmitters and receivers at each band. A prototype which implements multiband ambient backscatter across five bands is shown in Figure 4.2.

In addition to the enhanced reliability provided by frequency diversity, when multiple bands are excited this system also would allow ambient backscatter tags to transmit multiple channels of data simultaneously in many scenarios. Figure 4.3 shows the degree of isolation between different transmit-receive pairs for the five-band prototype, illustrating that independent communication can take place with only a small amount of crosstalk between channels.

Multiband backscatter fundamentally appears to be a viable solution, and it is certainly an academically interesting project with many avenues and challenges to explore. There is a potential for truly battery-less RF-powered nodes which communicate well in a wide variety of RF environments. However, it also has some drawbacks and significant challenges.

One significant hurdle in the practicality of multiband ambient backscatter is in extremely high system complexity. Many applications of ambient backscatter, such as in low-power and low-cost sensor nodes, do not warrant highly complex solutions. The added complexity means added cost and development time, nulling the benefits of selecting ambient backscatter over

		TX-TX Crosstalk (dB)				
		1	2	3	4	5
Transmit Band	5	-52.0	-52.0	-52.0	-52.0	0.0
	4	-51.9	-51.9	-45.9	0.0	-51.9
	3	-40.1	-24.6	0.0	-40.1	-44.6
	2	-15.9	0.0	-34.6	-38.5	-45.9
	1	0.0	-26.9	-32.6	-41.4	-47.4

Figure 4.3: An indication of how well isolated transmit bands are from each other in a five-band multiband ambient backscatter prototype.

conventional radio in many cases.

Another significant hurdle is shared by other types of ambient backscatter systems: Low sensitivity at the receiver. Because receivers are passive and ultra-low power in these systems, good sensitivity is difficult to attain. Some work has shown ultra low power wakeup radio type systems which have high sensitivity, but these systems are configured to convey only one bit of information to a receiver; whether it should wake or not[36]. Conveying more data requires a different set of design goals and may be hard to achieve at high sensitivity in a passive receiver.

An alternative strategy could be automation in tuning (“agile harvesting). However, an efficient tunable harvester or passive receiver requires a high degree of complexity in circuit design, resulting in a solution which is both larger and more expensive to build and thus less practically applicable. To our knowledge, a high efficiency tunable harvester has not yet been shown in published literature.

Thus neither auto tuning / agile harvesting or multiband backscatter are near-term solutions in a system where the primary value propositions would be low cost and simplicity of deployment.

These drawbacks and hurdles presented a challenge to come up with something better.

The following section introduces a different topology which maintains much of the simplicity of classical ambient backscatter while also implementing frequency diversity.

#### *4.1.3 Wideband Ambient Backscatter*

Multiband and classical ambient backscatter share the issue of receiver sensitivity, and while multiband backscatter partially solves the single-source fading issue, it does so at the cost of very high complexity. In the rest of this chapter, we consider another method which can solve single-source fading.

We begin by examining assumptions about the system. Whereas classical ambient backscatter is done in a tag-to-tag manner on completely passive tags, many applications do not require this. If we are to relax the requirement for tag to harvest energy it needs from the RF signal, and if we allow a powered receiver, theres another interesting avenue to explore:

**To address this issue of pervasive operation across geographical location, without increasing the complexity of the transmitter, we propose wideband ambient backscatter as a viable solution. In wideband ambient backscatter, a single backscatter transmitter connected to a wideband antenna can scatter simultaneously across any energy-carrying spectral band.**

Wideband ambient backscatter can entirely eliminate the need for retuning or careful selection of operating frequencies at design time, and can provide the desired frequency diversity while maintaining a very low system complexity.

The advantage of wideband ambient backscatter is the simultaneous use of any and all available radio power. This means that any location with sufficient power in *any* band will allow operation of the transceiver, greatly expanding the coverage area.

Of course, the tradeoff here is that the receiver is now assumed to be a conventional, powered radio receiver with LNA, mixer, local oscillator, and baseband processing, and therefore the receiver no longer adheres to the ultra-low power constraints of a passive system. Because of this, the most suitable applications for wideband ambient backscatter include star-

topology sensor networks with the hub node acting as gateway or aggregator, where the hub is implemented by a powered conventional radio receiver.

During the recent course of this work, results of an independent but very similar project were published by Chouchang Yang et. al., at Disney Research[50]. The underlying concept, that of scattering at any and all frequency bands simultaneously, is identical to what we present here. However, details of the implementation and system performance differ significantly, most notably in the lack of a subcarrier in the method of [50], and thus we feel this work still provides significant additional contribution to the state of the art in ambient backscatter.

## **4.2 Design**

Wideband ambient backscatter differs from both conventional backscatter and multiband backscatter in that no particular frequency band is targeted. The scatterer simply intends to re-radiate across a very large bandwidth, with the hope that there are plenty of ambient signal sources contained in that bandwidth.

Design targets for the wideband ambient backscatter system include the following:

- In order to take advantage of as many ambient signal sources as possible, the transmitter must be effective at re-radiating energy across a very large bandwidth. For instance, the entire UHF band from 300 MHz to 3 GHz.
- The receiver must be able to efficiently identify bands on which to listen for the transmitted data.
- Because host signals are modulated, protocol design should be such that fluctuations in the amplitude or phase of underlying host signal(s) do not significantly impact reception of the ambient backscatter signal.

In this section we describe how these goals can be achieved, splitting our discussion into three parts to focus on the transmitter, the receiver, and the protocol design in turn.

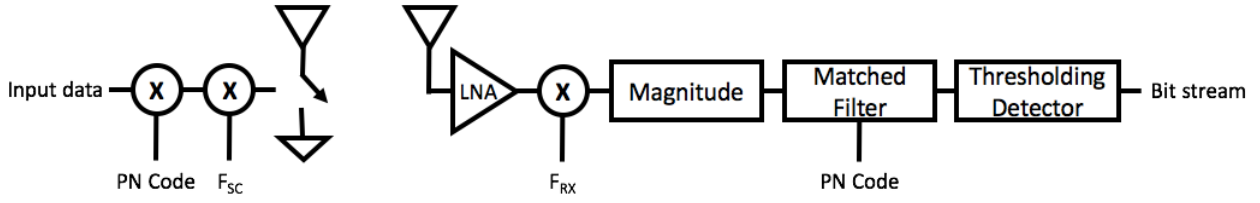


Figure 4.4: The complementary transmit and receive architectures for the proposed wideband ambient backscatter system.

#### 4.2.1 Transmitter Design

A diagram of both the transmit and receive architecture is given in Figure 4.4.

The phase of the reflected signal is modulated by a wideband switch. The switch is configured to allow transitions from an open state to a short state. Because the bandwidth is large, no particular impedance target can be achieved for either the open and short states, as a matching network capable of producing that effect is not feasible[14]. Instead, we simply design the system to target a 180 degree change in reflected signal phase between the open and short states for each particular frequency. Also note that reflection phase transitions in a backscatter system are capable of producing a larger contrast in signal observed at a receiver than are reflection magnitude transitions.

$$\Gamma = \frac{Z_L - Z_S}{Z_L + Z_S} = \frac{Z_{\text{ANTENNA}} - Z_{\text{SWITCH}}}{Z_{\text{ANTENNA}} + Z_{\text{SWITCH}}} \quad (4.1)$$

$$\begin{aligned} \Gamma|_{Z_{\text{SWITCH}}=0} &= 1 = 1\angle 0^\circ \\ \Gamma|_{Z_{\text{SWITCH}} \rightarrow \infty} &= \lim_{Z_{\text{SWITCH}} \rightarrow \infty} \Gamma = -1 = 1\angle 180^\circ \end{aligned} \quad (4.2)$$

Equation 4.2 describes the optimal reflection coefficient of the switch in the open and shorted states. Transitioning from an open to shorted state produces the largest change

possible in the reflection coefficient. In the general case this in turn produces the largest change in radar cross section ( $\Delta\text{RCS}$ ) of the antenna, resulting in the largest amplitude re-radiated signal possible for an un-amplified backscatter device.

Because the underlying signals over which we are communicating are already modulated, and in many cases this modulation can interfere with our communication channel, it is desirable to move reflected energy away from the frequency band of the underlying signal source. We do this by introducing a subcarrier on the transmitter.

The transmitter in this system is extremely simple and doesn't require much thought towards careful design. This is a huge positive in real deployments; the requirement for extensive design and high complexity drive up cost and make large scale deployments unreasonable.

#### *4.2.2 Transmit antenna*

The wideband ambient backscatter tag is connected to a wideband antenna. The device uses a switch configuration which can backscatter across the entire bandwidth of the antenna.

The antennas characteristics and particularly its operating bandwidth and efficiency are one of the key defining factors in the overall performance of the system. That said, the particulars of antenna band are not overly important; the main criteria for selection of the antenna is that it is designed to operate in a band in which significant ambient energy is available. In our system, we target VHF (30-300MHz) and UHF (300MHz-3GHz) bands, and thus choose antennas which are passable in these frequency ranges.

#### *4.2.3 Receiver Design*

In a classic tradeoff, the receiver is made more complex than in a classic ambient backscatter system. A powered receiver with a front end capable of tuning across a very wide range is used. This receiver is coupled to its own wideband antenna, and used to target frequencies across the VHF and UHF bands.

The receiver does not intend to capture energy from all bands simultaneously; instead, the goal is for the receiver to perform an intelligent search, identify bands which are likely to be useful for receiving data from the wideband scattering transmitter, and tune to find these bands.

The optimal bands for reception will be quiet bands spaced at the subcarrier frequency  $F_{SC}$  apart from very loud bands. Thus an intelligent search could scan power spectral density across the entire bandwidth of the receiver and identify optimal candidate reception frequencies based on this criteria.

Because the signal is processed non-coherently, and with a disregard for phase and frequency information (data is encoded by the presence or absence of energy in the band  $F_{SC}$  distant from the host signal), the receiver does not need to sample at the bandwidth of the host signal. In fact, the sample rate need only be at or above the Nyquist rate for the data signal itself. This is in stark contrast to other work in powered receivers targeting ambient backscatter transmitters, in which bandwidths of hundreds of MHz were captured and processed. This means a drastic reduction in signal processing complexity over systems which need to capture at or above the host signal bandwidth.

#### *4.2.4 Scanning algorithm*

A simple algorithm for the scanning procedure was developed and used in all system testing.

Periodically, receive frequency candidates are forward-computed based on power spectral density information. This list of all possible receive frequencies is then separated into a whitelist, graylist, and blacklist, where the whitelist contains frequency candidates on which data has recently been received, the graylist contains candidates on which no data has yet been received, and the blacklist contains frequencies which were not selected as candidates based on a periodic spectral examination. When in scanning mode (e.g., when no data is actively being received from the intended source), the receiver usually tunes to the whitelisted frequencies in a round-robin fashion, but at random intervals it will instead tune to one of the graylisted or (less frequently) to blacklisted frequencies to determine if anything has

changed.

The power spectral density map which is used to periodically update the candidate list is updated every time a channel is scanned, so it stays current over time.

### **4.3 Modulation and Protocol**

The goal of the modulation method and protocol design is to reject fluctuations in the underlying ambient signal, such that our system can still operate in the adverse environment of a highly modulated host signal.

Two strategies towards achieving this are employed. In the first, a subcarrier is used to move re-radiated energy outside the bandwidth of the host signal, so that our weak scattered signal is not contending directly with the host signal itself. In the second, a standard DSSS channel coding scheme is implemented, and the process gain associated with cross-correlating for long codes at the receiver provides a means of further rejecting noise induced by host signal fluctuations.

#### *4.3.1 Frequency plan*

A subcarrier is added to modulated data in order to push the re-radiated signal outside the spectral band of the host ambient signal. It is thus optimal that the subcarrier frequency is chosen to be large enough to provide for no overlapping region between the host signal and the scatterers re-radiated signal. Figure 4.5 depicts the frequency plan for the system. For an ATSC digital television signal, where signal bandwidth is approximately 6MHz, an appropriate subcarrier would need to be chosen at or above 6MHz in order to prevent this overlap.

In [37], a discrete-time model for non-coherent detection of ambient backscatter is given. In the propagation model used by Qian et. al., duplicated here in Equation 4.3,  $h_{sr}$  is the channel from ambient source to receiver,  $h_{st}$  is the channel from ambient source to backscatter transmitter,  $h_{tr}$  is the channel from backscatter transmitter to receiver,  $b_k$  represents the data symbol currently being transmitted by the scatterer,  $s[n]$  is the host's transmitted signal,  $\alpha$

represents a fixed complex attenuation arising from the backscatter operation and antenna parameters, and  $\omega[n]$  captures any external noise or interference.

$$y[n] = (h_{sr} + \alpha h_{st} h_{tr} b_k) s[n] + \omega[n] \quad (4.3)$$

Our proposed wideband ambient backscatter system introduces a subcarrier to move the backscattered spectrum out of the bandwidth of the host signal and into its own spectral region. Backscattered energy appears on two bands,  $F_C + F_{SC}$  and  $F_C - F_{SC}$ , representing the results of mixing the subcarrier at  $F_{SC}$  with the host signal at  $F_C$ .

Because the receiver listens at only one of the two image frequencies, and because the image bands don't overlap with the host band, the receiver will not be subjected to the unmodulated host signal. Additionally, the signal seen at the receiver will contain only half of the power of the backscattered signal (the other half being at the opposing image frequency). Equation 4.4 modifies the model from Equation 4.3 to accommodate this new topology.

$$y[n] = \frac{1}{\sqrt{2}} \alpha h_{st} h_{tr} b_k s[n] + \omega[n] \quad (4.4)$$

Note that in typical deployments, the ambient-source-to-receiver channel coefficient  $h_{sr}$  will be much larger in magnitude than the product of source-to-scatterer and scatterer-to-receiver coefficients  $h_{st} h_{tr}$ , and thus the host signal  $h_{sr} s[n]$  present at the receiver will be a major source of interference for our detector. Getting rid of this term by pushing energy out of the band of the host signal results in a much cleaner and higher SNR link.

### *Single Sideband Backscatter*

It is worth noting that a prior publication on backscatter systems[17] yielded a single-sideband modulated scatterer; that is, one which can use a subcarrier to produce only a single image of a host signal rather than the typical two-image reflection ( $F_C + F_{SC}$  and  $F_C - F_{SC}$ ). While this technique provides a 3 dB improvement in link budget in theory, unfortunately

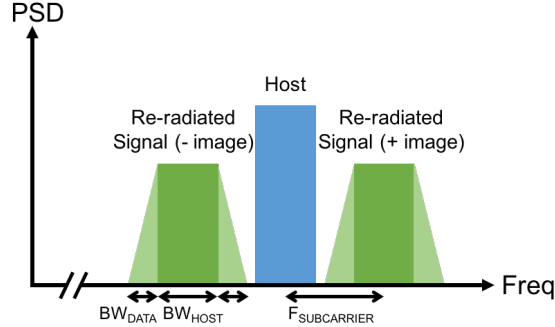


Figure 4.5: Frequency plan for subcarrier-offset wideband ambient backscatter, showing the original host signal and the re-radiated signal produced by the tag.

it cannot be implemented in the wideband ambient backscatter system. This is because impedance matching limits (described by Fano in [14]) prevent specific load impedance relationships from being maintained across a wide bandwidth. Thus any wideband ambient backscatter system employing a subcarrier will need to produce two image frequencies.

#### 4.3.2 Coding and Packet Structure

A DSSS coding scheme is implemented, employing Gold codes which are generated by the XOR'ing of the output sequences of two maximal-length linear feedback shift registers (LFSR) of the same bit depth. Use of Gold codes allows proven properties to be leveraged; Gold codes have been shown to have good autocorrelation properties, and codes within the same family (same two generator LFSRs but differing pattern offsets) have good cross-correlation properties.

Longer codes result in more process gain; the gain inherently provided by cross-correlation. The process gain is equal to the energy in the code, as shown by the expression for SNR in a cross-correlating receiver given in Equation 4.5 taken from a popular RADAR signal processing textbook [40], where  $E_s$  is the energy in the code and  $\sigma_n^2$  is the noise power.

$$\text{SNR}_{\max} = \frac{E_s}{\sigma_n^2} \quad (4.5)$$

There are two distinct rates which are present in this system, the chip rate and the data rate. The chip rate is the rate at which new PN symbols are shifted onto the output multiplier, while the data rate is the rate at which new data symbols are provided. In a classical implementation, the chip rate will be greater than the data rate by a factor of the length of the code.

A very simple packet structure is adopted. First, a 16-bit preamble signals the start of packet to the receiver. Next comes a length field, followed by the data field it measures. Lastly, a 16-bit CRC is included to allow packet-level correctness to be evaluated.

#### *4.3.3 Multi-user Capability*

One unfortunate limitation of wideband ambient backscatter is that all transmitters scatter energy on all bands at once, with no ability to discriminate between different sources of ambient energy. Therefore, different bands may not be used to encode data intended for different receivers in the same way as is done in conventional multi-channel radio networks.

However, we can still leverage several degrees of separation from both natural spatial diversity and parameters in the system to achieve simultaneous multi-user operation.

The first of these degrees of separation is multipath fading of the ambient signal itself; the very thing we are trying to solve by using wideband ambient backscatter can in fact be an important source of diversity when considering multi-user deployments. Spatial fluctuations in power density of ambient sources results in different scatterers having different frequency transmission profiles, providing some amount of isolation (which is hard to characterize as its highly dependent on the characteristics of the channel and depth of fading). Evidence of this diversity can be seen in Figure 4.13(b), in which different transmitter locations resulted in different selected operating frequencies.

Another degree of separation between users is the PN sequence chosen by the DSSS

transmitter. Different nodes may use different PN sequences, for instance different Gold codes from the same family. For instance, a 63-bit Gold code has 62 different family members of which none will produce significant interference in the cross-correlating receiver.

Yet another degree of separation is the subcarrier frequency selection. Different subcarrier frequencies could feasibly be used by different nodes to transmit data orthogonally.

There are many problems around coordination of nodes in a network, and how to best leverage all of the degrees of separation given above. Without any form of downlink (data transmission to nodes) a specific MAC strategy for coordinating which codes to use, which subcarrier frequency to use, and when to transmit will be hard to form. However, even a random walk through different code-subcarrier pairs should suffice for reducing or preventing collisions in many applications.

#### ***4.4 Prototype implementation***

To better understand the real-world performance and practicality of the system, a prototype of both the transmitter and receiver were constructed.

The transmitter, pictured in Figure 4.6, is very simple and has only two essential components: a low-power MSP430F5310 microcontroller, and a backscatter switch. The MSP430F5310 was selected for its low power clock synthesis capability in the form of a frequency-locked loop (FLL), which is employed to generate arbitrary subcarrier frequencies. The switch, an HMC550A from Analog Devices, was selected for its wide (6 GHz) bandwidth, fast switching times, and low ON resistance.

The antenna for the transmitter is a wideband UHF monopole which is normally sold and used with TV tuner cards. No careful antenna testing was done as that was not the focus of this project. However, in our experimentation, this small monopole was capable of reasonable pickup from least 100 MHz to 1 GHz.

Figure 4.9 depicts the measured reactive impedance at the port of the tag as a function of frequency. The top and bottom trace depict the open and short states of the switch, respectively. Note that an shorted or open switch does not always translate to a pure short

or pure open circuit impedance; rotation is introduced by electrical length in the switching apparatus, and that rotation is a function of frequency. Thus a tag impedance fluctuation nearly sinusoidal in wavelength is introduced.

A simple firmware stack was constructed to allow transmission of arbitrary packets following a simple packet structure (source address, sequence number, payload, CRC). The firmware leverages features of the MSP430s clock synthesis module to generate subcarrier frequencies, bringing the generated clock out to a transmit pin and then modulating it with baseband data. Mixing in of the PN code sequence is also handled by this firmware set.

The hardware portion of the receiver is implemented by a popular and inexpensive RTL-SDR software defined radio (see Figure 4.7. This bus-powered USB dongle radio, while not as capable as the research-oriented USRP series devices, is around one hundredth the cost and thus easy to imagine being used in real-world deployments. The receiver made use of the same UHF monopole antenna as the transmitter, which actually ships with the RTL-SDR unit pictured.

Signal processing and high-level receiver logic is implemented around gnuradio, a toolkit for implementing software defined radio applications. There are two components to the receiver: a gnuradio flowgraph which handles signal processing and bit detection, and a high-level logic module which handles frequency scanning according to the method outlined in Section 4.2. The ZeroMQ sockets layer is used to interface these two blocks, as they are each written in different languages and have to run within the confines of the sometimes arcane gnuradio framework.

A visual depiction of the flowgraph used to implement signal processing is shown in Figure 4.8.



Figure 4.6: Prototype of the wideband ambient backscatter transmitter. The antenna used is a compact, fairly low efficiency monopole designed for reception of TV signals in the 400-900 MHz range. In our experiments this antenna responds sufficiently down to around 100 MHz. The tag itself is composed simply of a TI MSP430F5310, an HMC550A wideband RF switch, and a 20mm coin cell battery.



Figure 4.7: This popular and inexpensive (about 20 US dollars) implementation of the RTL-SDR software defined radio is used in all experiments. This radio is capable of tuning across a range of 30 MHz to 1.3 GHz, and are thus well suited to pick up re-radiated energy from the tag in FM radio bands, TV bands, at frequencies used for industrial / scientific / medical applications, and cellular base station and mobile transceiver transmission frequencies. The ADC resolution of the radio is 8 bits, and the sampling rate may be varied from 1 to 3 MHz.

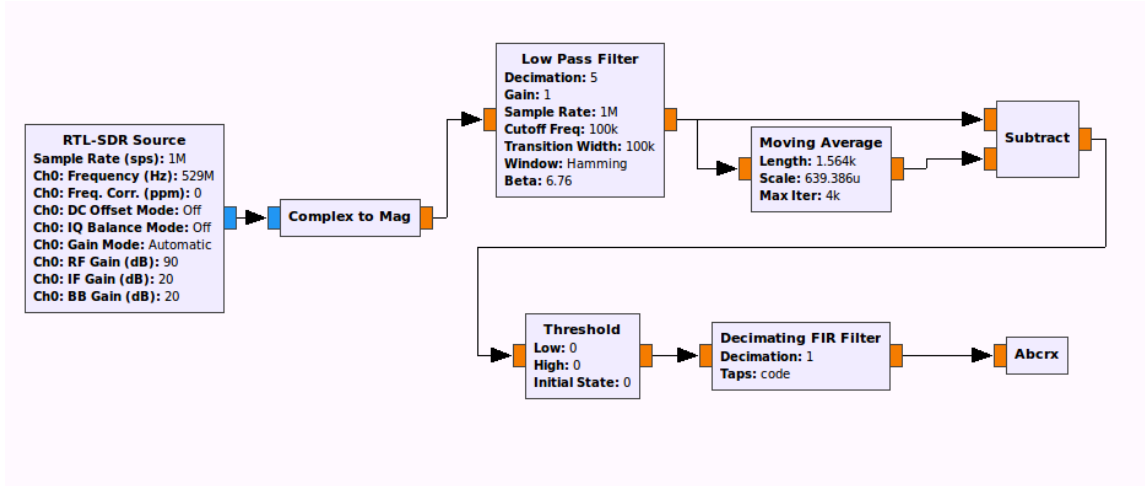


Figure 4.8: Graphical version of the gnuradio flowgraph implementing the correlating receiver. A matched filter is used to identify the presence of the PN sequence in the input signal. The Abcrx block is a custom out-of-tree module which does bit detection, passing detected bits to a python program which decodes packets and manages frequency scanning.

## 4.5 Experimental results

To characterize the wideband ambient backscatter system, several tests were done both at the level of individual system components and of overall performance.

### 4.5.1 Backscatter Capability

The key factors in the ability of the tag to perform backscatter are the contrast in the degree of mismatch that is produced between the tags RF port and its antenna, and the details of the radar cross section of the antenna. Because in this work we choose to de-prioritize the design of the antenna, we will only discuss the impedance mismatch contrast that the tag can produce.

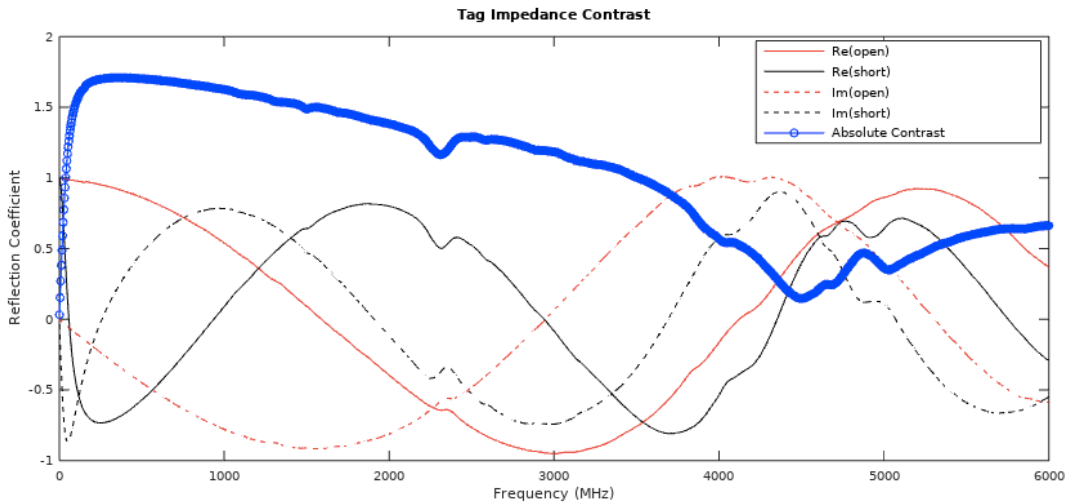


Figure 4.9: Measured real and reactive components of impedance at tag port, from 1MHz to 6GHz, for both open and short states. The heavy blue line shows the absolute contrast (vector distance) between open and short states.

Assuming a 50 Ohm antenna impedance, Figure 4.9 illustrates the real and reactive parts of measured reflection coefficient produced when connecting the antenna to the tags RF port, for each of the two positions of the switch (open and short). Note that there is significant

rotation in the impedance of an open and short value as a function of frequency, but that what matters is the contrast between those two states (displayed on the plot as a heavy blue line). The best contrast achievable in a passive system would be 2.0, that resulting from a 180 degree phase shift between open and short in a completely lossless system. Our system achieves performance near to this ideal case across much of the frequency range.

Fortunately, producing this contrast is not difficult from a design perspective; in our design, the switch connects directly to the antenna port with as little electrical length as was achievable on a PCB, and this produces the near-optimal performance seen.

#### *4.5.2 Communication Performance*

Tests were done to characterize the performance of packet transmission and reception. In this first set of tests, the receiver was placed at a fixed position in a ground level outdoor location with low ambient signal strength (typical carriers range from -85 to -65 dBm at the receiver antenna port). The distance between the transmitter and receiver was varied, while the transmitter sent 7-byte packets at a 1kbps data rate using 63 PN sequence chips per bit (chip rate of 63kHz). The subcarrier frequency was 10 MHz, easily accommodating the typical 6 MHz bandwidth of television signals which were the predominant form of ambient signals captured by the wideband UHF antenna. Four suitable frequency bands were chosen by allowing the receiver to scan all available frequencies in the 100 MHz to 1 GHz bandwidth, and the receiver was then configured to resolve packets on a single frequency for some duration and compute a packet error rate (PER).

Figure 4.11 depicts the results of this experiment, in which the four bands were compared in terms of PER at various TX-RX distances. The dotted black line illustrates the result achievable by switching to the most suitable band at each location, the goal of the scanning algorithm presented in this work.

Two of the bands, 549 MHz and 529 MHz, are both a 10 MHz offset from a 539 MHz carrier, the most prominent signal source at this location being a TV broadcast at 539 MHz.

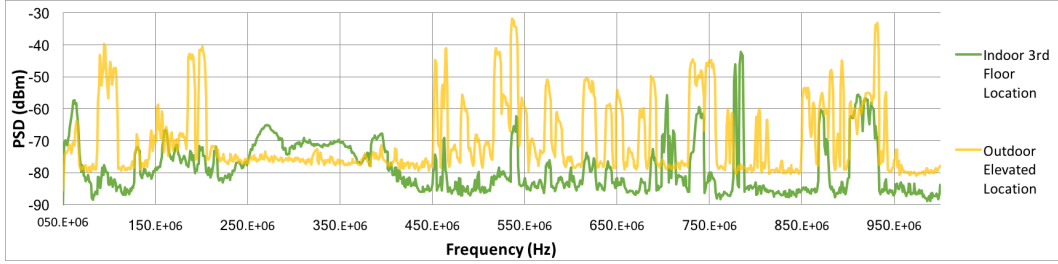


Figure 4.10: Power spectral density in the 50 MHz to 1 GHz range for the two primary indoor and outdoor test locations, within several hundred meters of each other. Note that, in general, the outdoor location experiences much higher ambient power availability.

It is worth noting that in some cases, the  $F_C + F_{SC}$  and  $F_C - F_{SC}$  images produced by the backscatter operation are not equivalent in suitability for reception of the backscattered signal. This happens either when other adjacent ambient sources overlap with one of the image bands, or when the image bands are subjected to differences in multipath diversity due to slightly different wavelengths. In either case, the performance of the two image bands may be different. In this experiment, we observe several data points at which the two image bands significantly differ in PER.

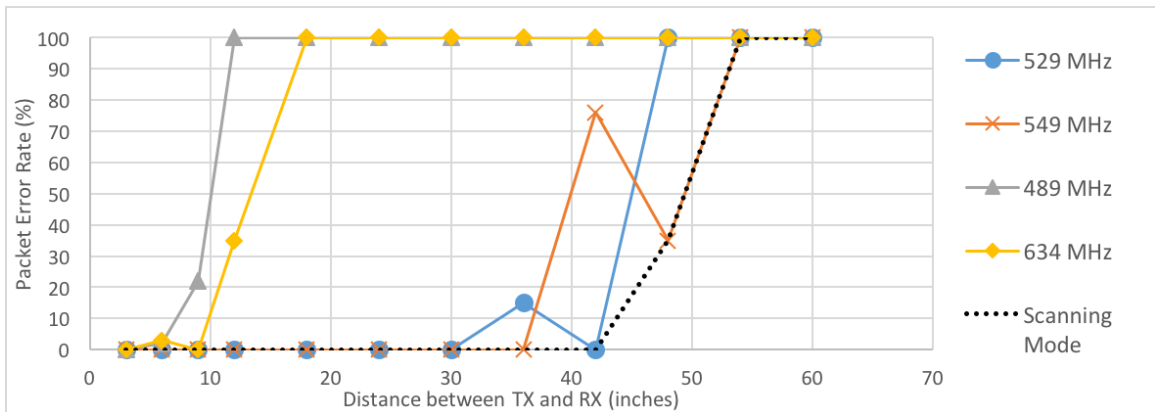


Figure 4.11: PER as a function of range for an outdoor scenario with low incident power at ground level, with several traces representing different receive frequencies.

#### 4.5.3 Frequency Agility

The next set of results explores the systems ability to operate over a wide area by automatically tuning to the most suitable operating frequency at each test location.

A 6th floor balcony of a University office building was selected, where due to the exposed location a plethora of strong ambient signals could be observed.

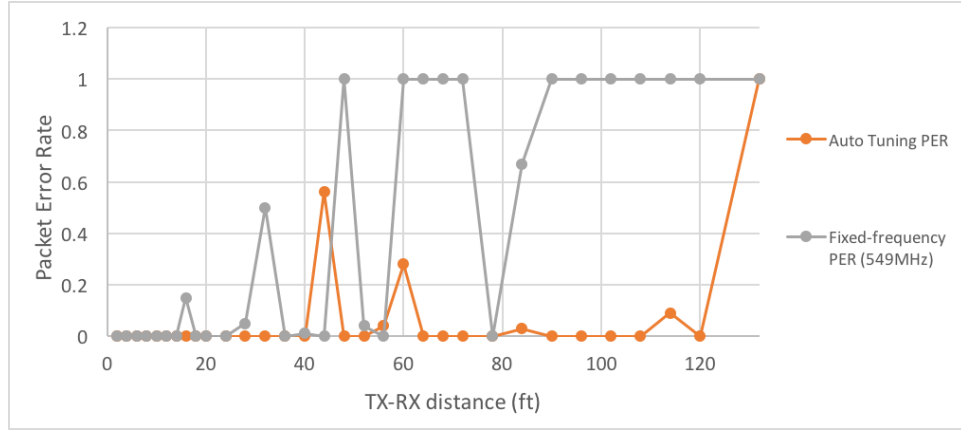


Figure 4.12: The 6th floor balcony location used in frequency agility testing.

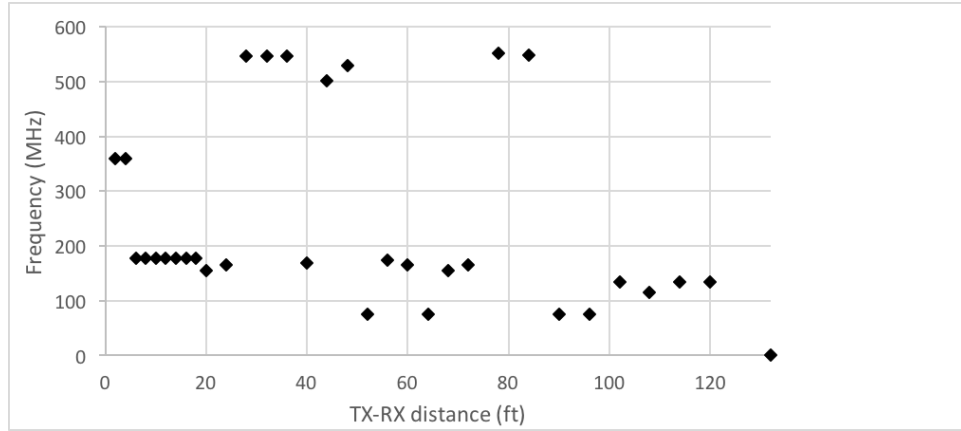
The receiver was placed at a fixed location on the outer railing of the balcony, see Figure 4.12. The transmitter was moved along the railing, and at each transmit location some time was allowed for the receiver to search and retune to an appropriate frequency for reception. The same 64 chip sequence and 1 kbps data rates were used as in the prior experiment. Results are shown in Figure 4.13.

In Figure 4.13(a), the packet error rate is given as a function of position for both an

auto-tuning receiver and a single-frequency reference receiver centered at 549 MHz. The receive frequency chosen by the auto-tuning receiver for each test position is also reported in Figure 4.13(b).



(a) Packet Error Rate



(b) Auto-Selected Receive Frequency

Figure 4.13: Tag and receiver were placed a varying distance apart in an elevated outdoor location, and the automated frequency selection algorithm was allowed to determine a suitable operating frequency at each location.

The choice of a 549 MHz receive frequency for the reference receiver was due to the existence of a very prominent 539 MHz signal, transmitted by a television broadcast tower

only 4.2 km distant from the balcony on which the experiments were run, and having a clear line-of-sight path to the balcony. Earlier work presented in Chapter 3 of this thesis identified this as a good candidate band for ambient backscatter communication on this particular balcony. The purpose of choosing this particular frequency as a reference is to demonstrate that, even with a very prominent ambient source, a single-frequency system has severe range and reliability reduction when compared with the intelligent frequency-agile receiver system shown in this chapter. These reliability issues come mostly from fading effects in the channel, which produce localized nulls and can be overcome with frequency diversity.

Due to the greater intensity of ambient signal strength as compared with the indoor scenario, operation was sustainable at up to an 120 foot range from transmitter to receiver, and in the case of the frequency-agile receiver every location attempted between 2 and 120 feet was successful in achieving less than about 60% packet error rate. This is in contrast with the fixed-frequency receive testing targeting the prominent nearby television broadcast signal, which only exhibited reliable operation at up to 44 feet, after which large null response areas were seen and eventually a total loss of signal occurred beginning at 90 feet.

The lack of excessive repetition in the frequency chosen by the frequency-agile receiver also validates the method as compared with single-frequency ambient backscatter by showing that the receiver actually lost signal and was forced to switch frequencies multiple times as the transmitter was moved.

It is also noteworthy that while the most prominent ambient signal source in this RF environment was a TV broadcast tower 4km away and transmitting at 539MHz, the system favored this carrier for only seven of the 32 test locations. The fact that this 'strongest' signal was not often selected is further evidence that even the prominent signal encountered significant fading.

#### 4.5.4 Quality of Service Testing for an Indoor Application

A simple quality of service test was designed in which a wideband ambient backscatter transmitter and SDR-based receiver were placed at a 2 ft distance on a rolling cart as shown in Figure 4.14, and moved to each of 74 different test locations throughout 6 different floors of an office building, including two subterranean basement floors.

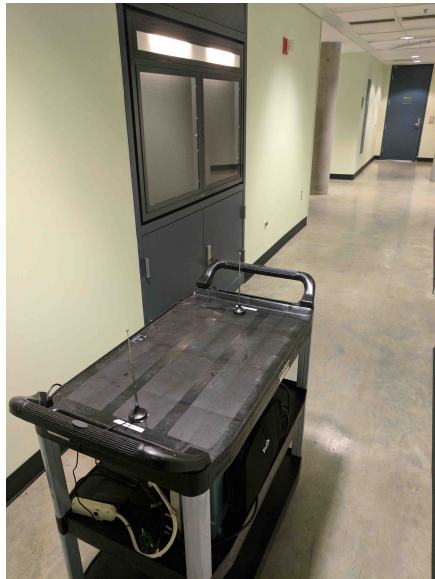


Figure 4.14: Test setup for indoor quality-of-service testing, with antennas separated by 2 ft on a rolling cart.

Packet error rate was measured at each of the test locations. The goal was to determine how many of the locations achieved an acceptable level of performance. Figure 4.15 illustrates the test locations on each floor of the building, with points color coded by PER. Auto-selected receive frequencies are also listed.

Because performance requirements vary between applications (e.g., a computer mouse needs very low PER due to latency requirements, while a room temperature sensor can generally accommodate higher PER), no hard threshold was set on PER, but rather measurements



Figure 4.15: Quality of Service Testing across six floors of an office building, including two subterranean basement floors. Transmitter and receiver were placed at a fixed separation distance of 2 ft at each test location. Link frequency was 1 kbps for each test, with a PN sequence length of 63 and a subcarrier frequency offset of 10 MHz.

are categorized and colored in the results plots based on whether they showed no errors at all (green), showed less than 10% packet error rate (yellow), or showed between 10% and 83% packet error rate (orange).

Figure 4.16 shows a CDF of packet error rate for the 74 different test locations shown. We can see that 54% of the test locations did not exhibit any packet loss in a 100-packet transmission, for a projected PER of under 1%. None of the locations tested exhibited packet error rates of greater than 83%, showing that short range communication is very achievable even within a large office building.

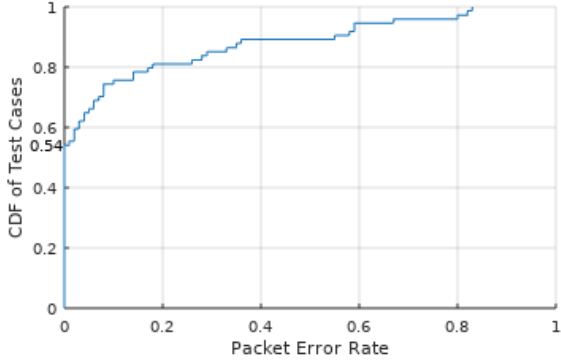


Figure 4.16: Cumulative distribution function of packet error rate across 74 test locations in an office building

#### 4.5.5 *Quality of Service Testing for an Outdoor Application*

The same type of quality of service test was performed in an outdoor scenario, with antennas attached to the roof of a car at a fixed distance of 6 ft, and the car driven throughout urban and suburban neighborhoods of Seattle.

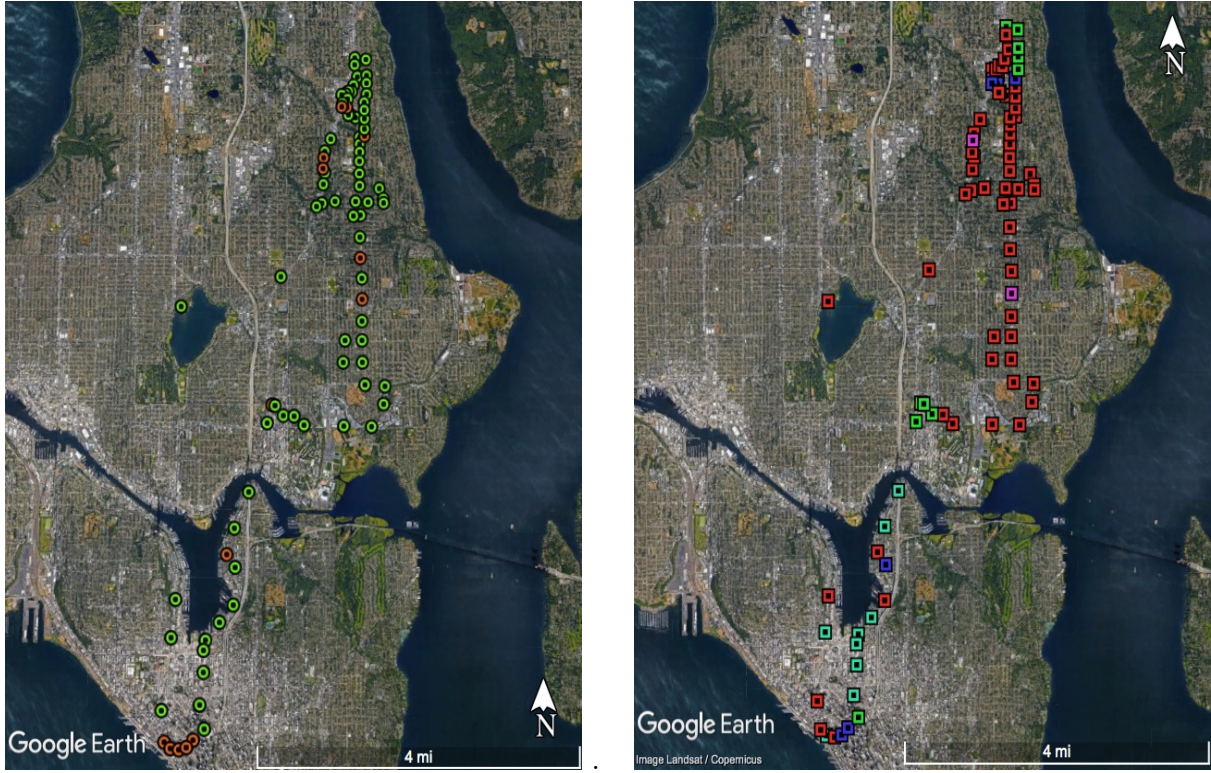
For each test location, the car was parked briefly to allow the receiver time to seek out a suitable receive frequency as needed and to allow error rate readings to stabilize<sup>1</sup>. Packet error rate (over a 100 packet transmission) and frequency of operation were recorded.

Results are shown overlayed on satellite imagery in Figure 4.17. Figure 4.17(a) illustrates packet error rate across test locations, while Figure 4.17(b) gives a feel for the way the frequency-agile receiver selected different frequency bands at different locations. Figure 4.18 shows a cumulative distribution function as a function of error rate across the 87 locations tested.

There were no test locations of the 87 attempted which resulted in total packet loss; the receiver was able to receive packets from the transmitter at all locations, with 66% of the locations experiencing no lost packets out of 100 attempted (for a projected PER of <1%).

---

<sup>1</sup>Anecdotally, in most cases the receiver did not require this dwell time and had settled on a suitable frequency while the car was still in motion.



(a) Packet Error Rate. Green indicates <1% error and orange, >77% (b) Auto-Selected Frequency, each color represents a unique frequency.

Figure 4.17: Quality of service testing across 87 outdoor locations in various neighborhoods of Seattle, Washington. TX and RX were placed at a 6ft separation on the roof of a car and driven to each test location.

#### 4.5.6 Power Consumption of Tag

While highly un-optimized and using entirely commercial off-the-shelf hardware, the power consumption of our system can still be compared very favorably against conventional radio transmitters. While transmitting, our commercial off-the-shelf prototype consumes a steady 2.0 mW when using a 10 MHz subcarrier frequency and 64 kHz chip rate. It is foreseeable that a 10x or larger improvement in power consumption could be achievable with an application-specific integrated circuit.

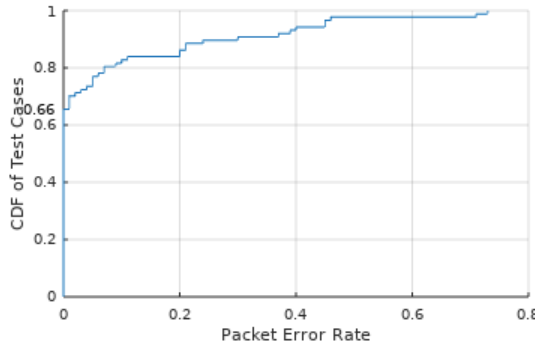


Figure 4.18: Cumulative distribution function of packet error rate across 87 outdoor test locations with a 6 ft TX-RX spacing

#### 4.5.7 Notes on Computational Burden of Receiver

In all of the above tests, receiver sampling rate was set to the minimum of 1 MHz, and further downsampled to 200 kHz before decoding to further ease the computational burden. Packets were decoded live by our script, and frequency tuning was also done live in real time and unaided by human intervention. Typical scanning/retuning times were 2 seconds to 60 seconds. The reported CPU usage of a Intel Core i5 laptop running Ubuntu 16.04 was 5-7% when running the receiver application.

## Chapter 5

### PRIOR ART

There is a significant amount of existing and ongoing work in the area of utilizing ambient signals to the advantage of connected devices, spanning at least a decade. Further, there is a much longer history of use of backscatter techniques in low power radio communication devices. In this chapter, we do not exhaustively cover the field of ambient RF harvesting but instead provide a brief review of existing work in wideband/multiband RF energy harvesting/scavenging. We then go into a detailed review of existing work in modulated backscatter communication and ambient backscatter systems.

Much of this work has arisen concurrently with our own. In some cases, work by other groups has been inspired by our work, particularly in the case of ambient backscatter. In other cases, we have been partially inspired by others' work.

#### **5.1 Wideband / Multiband RF Energy Harvesting and Scavenging**

Some work has been done on wideband harvesting[15], tunable harvesting[44], and multiband harvesting[21, 30]. While wideband harvesting can capture energy across a large swath of spectrum, it typically results in very low efficiency at any particular source frequency as the quality of the impedance match between the antenna and single rectifier must reduce as the bandwidth increases[14].

Tunable harvesting allows a system to dynamically select a band of interest based on spectral availability, and therefore promises to be able to provide efficient rectification of signals from a single source, regardless of the frequency of that source. However, tunable harvesters in battery free systems will require solving the very difficult bootstrapping problem to allow the system to cold-start, and also will ignore energy outside the band to which they

are tuned. To add to this, tunable circuit elements such as varactors can have significant impact on the efficiency of harvesting systems. Very few tunable systems have been shown in literature, probably due to the difficulty of constructing this type of system.

## **5.2 Communication by Backscatter Modulation**

Harry Stockman's seminal 1948 article in the Proceedings of the IRE (predecessor to the IEEE) described his experiments with rotating retroreflectors, which would produce a tone in a radio receiver when power was beamed at them. These methods inspired a new communication paradigm in which energy is beamed at a distant target which then reflects (scatters) that energy in such a way as to convey information to a listener stationed at the beams source.[46]

Modern systems seen across industrial, commercial, and consumer use which employ these techniques include are classified and described in this section.

### *5.2.1 Systems using Backscatter of Intentional Sources*

There are a variety of both commercially available and research systems which employ backscatter of intentionally provided energy. The following list describes the categories of these systems as they currently exist:

1. **UHF RFID systems.** These systems employ a reader (interrogator) which acts as both carrier emitter and receiver. Tags are often passive.
2. **Bistatic Backscatter.** These systems, seen in research, use an architecture in which carrier emitter and receiver are spatially separated, and are often independent systems[22].
3. **High data rate QAM backscatter.** Expanding the constellation of impedance points used by the scattering device increases data rate, much as is done in conventional higher-order modulation transceivers[48].

4. **Passive Wi-Fi, BLE, and LoRa.** In these methods, shown in research, a backscatter device synthesizes conventional Wi-Fi, BLE, LoRa, or other protocols through modulated backscatter of a continuous wave or other signal. The resulting packets are then received and interpreted by a conventional Wi-Fi/BLE/LoRa receiver[20, 18, 12, 13, 17].
5. **Near field communication.** Though technically employing *load modulation* rather than backscatter, in these systems a passive or active tag signals to a magnetically-coupled reader by modulating the current through its receive coil. The very short range of this technique places it in a different application space than the methods presented in this work.

### 5.2.2 Systems using Backscatter of Ambient Sources

“Wi-Fi backscatter”.

A system which modulates scattering of existing unaltered Wi-Fi signals, resulting in a change in channel state which can be detected at an ordinary Wi-Fi receiver[19]. An enhancement on this concept shows that bit-level modulation is possible, increasing throughput dramatically[51].

*FM backscatter*

In this topology, normal FM radio stations are used as a carrier signal for a backscatter device (which like in this work uses a subcarrier to push the host’s signal into an adjacent unoccupied band). The backscatter device’s impact on the host signal is that of advancing or retreating the signal’s phase, which is easily detectable by conventional FM receivers in, for instance, smartphones[9].

### *Wideband Ambient Backscatter*

During the recent course of this work, a paper on a wideband ambient backscatter method was published by Dr. Alanson Sample’s team at Disney Research[50]. In Sample’s work, receiver complexity is taken to an extreme with an ultra-wideband receiver design employing multiple antennas and multiple high-bandwidth USRP X300 devices, capturing information across a 266 MHz bandwidth. The benefits provided by such complexity are clear; the authors of this work use a maximal ratio combining technique to take advantage of the diversity provided by many captured channels, detecting and decoding data based on a linear combination of the channels. This results in significant range enhancement, even at low ambient signal strength.

Our work differs from the work done at Disney Research in that our work makes use of a transmit subcarrier, which pushes scattered energy out of the band of the direct path energy from the ambient source. This leverages the receivers inbuilt channel filtering, thus eliminating nearly all of the interference imposed by the direct path from the ambient source. Because of this offset in frequency, we believe our technique suffers less from interference than an in-band ambient backscatter design would, thus reducing much of the need for techniques such as maximal ratio combining.

Additionally, our work makes use of a commodity radio receiver and needs only capture a 200 kHz to 1 MHz bandwidth in order to achieve information rates of 1 kbps, consuming only 5-7% of an Intel Core i5 laptop’s capacity to do this un-optimized decoding. This is in stark contrast to the system used by Sample, et. al, which employs a 266 MHz receive bandwidth captured by several thousand dollars worth of research-grade hardware, and would require extraordinary computing resources to achieve the live realtime decoding of packets necessary for a practical system.

#### *5.2.3 Passive Tag-to-Tag Communication*

Prior to our 2013 work published in SIGCOMM[24], which introduced ambient backscatter as a new communication primitive, there was no equivalent system in the literature that we are

aware of. However, one interesting piece of prior art came from Pavel Nikitin at Intermec. In this paper, it is shown that one RFID tag can talk to another by using backscatter modulation to emulate reader commands[28]. This was the first work we are aware of which demonstrates passive tag-to-tag communication.

A core challenge in passive tag-to-tag and ambient backscatter systems is low sensitivity at the receiver. Because receivers are passive and ultra-low power in these systems, good sensitivity is difficult to attain. This matches the challenges faced by wake-up radio receivers, which are used to wake connected devices usually with the intention of turning on a more power-intensive conventional receiver in preparation for an incoming transmission. Some work has shown ultra low power wakeup radio type systems which have impressive sensitivity, but these systems are generally configured to convey only one bit of information to a receiver; whether it should wake or not[36]. This is in contrast to ambient backscatter, in which transferring entire data packets is the objective. Thus some of the simplistic techniques used in wakeup radios may or may not be directly applicable.

#### *5.2.4 Subcarrier Modulated Backscasttter*

Existing work has also made use of a subcarrier, modulating the baseband signal applied to the backscatter switch, to push energy outside the band of the host signal and thus take advantage of the inbuilt filtering capabilities of the receiver's front end.

Ensworth et. al describe a system which synthesizes Bluetooth Low Energy (BLE) packets by modulated scattering of a continuous wave signal [12, 13]. Because the carrier emitter producing the continuous wave is a high intensity source and would interfere with reception of the resuling backscattered BLE packet, backscattered energy is pushed away from the incident wave frequency by use of a subcarrier.

Likewise, the “Passive Wi-Fi” and “LoRa Backscatter” systems of [20] and [47] make use of a subcarrier to move the backscattered Wi-Fi or LoRa packet away from the incident host signal, making it possible in the case of LoRa Backscatter to achieve hundreds of meters ranges.

Kimionis, et. al, describe a system in [22] which makes use of frequency shift keyed (FSK) backscatter transmitters in a bistatic arrangement; with carrier emitter and receiver spatially separated. Though these do make use of subcarriers, the receiver samples the entire bandwidth surrounding the scattered signal, including the carrier emitter frequency, and thus does not make use of it's inbuilt frequency selectivity to reject the carrier emitter's frequency.

In existing work which applies subcarriers to separate incident and reflected energy, the host signal (incident signal to be reflected) is an intentionally-provided source. In our technique, the host signal is an ambient and uncontrolled source which itself is modulated and carries information.

## Chapter 6

### SUMMARY AND CONCLUSION

Modern connected devices would benefit from practical ambient RF energy harvesting solutions. Two hurdles to achieving this exist. Firstly, the ability to achieve high harvesting sensitivity from multiple available bands must be achieved. Secondly, the power requirements of connectivity must be reduced in order to meet the power budget of an energy harvesting device.

In this work, a method for simultaneously and efficiently harvesting energy from multiple RF bands was introduced, meaning more power at more places is now accessible to RF harvesting devices.

Additionally, a communication system was designed and implemented which reflects ambient signals such as TV, radio, and cellular signals in order to send messages (rather than generating and emitting radio signals itself). This means the power required for devices to talk to each other, or to nearby access points or gateways, is significantly reduced.

Particularly, the wideband backscatter backscatter method presented here could produce a truly robust, extremely low-energy communication solution for IoT-class connected devices, potentially enabling those devices to operate without an energy depletion horizon and therefore without the associated battery replacement costs and inconvenience. The receiver simplicity in comparison with prior art lends itself well to mass installation.

In conclusion, we believe this work has made a measurable difference in the state of the art in low power connected devices by removing the requirement to frequently exchange or recharge batteries. This justifies more deeply embedded applications, and allows more numerous deployments of connected devices. The work presented here is a step towards allowing both long-lived and battery-free connected devices to be made a reality.

## BIBLIOGRAPHY

- [1] 8VSB vs. COFDM. [http://www.axcera.com/downloads/technotes-whitepapers/technote\\_4.pdf](http://www.axcera.com/downloads/technotes-whitepapers/technote_4.pdf).
- [2] Adg801-802 datasheet.
- [3] ADG902 RF switch datasheet.
- [4] Adxl362 datasheet.
- [5] Msp430g2x53 datasheet.
- [6] TS 881 datasheet, STMicroelectronics, july 2012.
- [7] Ieee 802.11g standard, 2003. <http://standards.ieee.org/getieee802/download/802.11g-2003.pdf>.
- [8] Ieee 802.21 standard, 2008. <http://standards.ieee.org/getieee802/download/802.21-2008.pdf>.
- [9] Fm backscatter: Enabling connected cities and smart fabrics. In *NSDI*, 2017.
- [10] J.L. Bohorquez, A.P. Chandrakasan, and J.L. Dawson. A  $350\mu\text{W}$  CMOS MSK transmitter and  $400\mu\text{W}$  OOK super-regenerative receiver for medical implant communications. *Solid-State Circuits, IEEE Journal of*, 44(4):1248 –1259, april 2009.
- [11] J.F. Dickson. On-chip high-voltage generation in mnos integrated circuits using an improved voltage multiplier technique. *Solid-State Circuits, IEEE Journal of*, 11(3):374–378, 1976.
- [12] J. F. Ensworth and M. S. Reynolds. Every smart phone is a backscatter reader: Modulated backscatter compatibility with bluetooth 4.0 low energy (ble) devices. In *2015 IEEE International Conference on RFID (RFID)*, pages 78–85, April 2015.
- [13] J. F. Ensworth and M. S. Reynolds. Ble-backscatter: Ultralow-power iot nodes compatible with bluetooth 4.0 low energy (ble) smartphones and tablets. *IEEE Transactions on Microwave Theory and Techniques*, PP(99):1–9, 2017.

- [14] Robert M. Fano. Theoretical limitations on the broadband matching of arbitrary impedances. Technical report, Massachusetts Institute of Technology, Research Laboratory of Electronics, 1948.
- [15] J.A. Hagerty, F.B. Helmbrecht, W.H. McCalpin, R. Zane, and Z.B. Popovic. Recycling ambient microwave energy with broad-band rectenna arrays. *Microwave Theory and Techniques, IEEE Transactions on*, 52(3):1014–1024, 2004.
- [16] Daniel Halperin, Ben Greenstein, Anmol Sheth, and David Wetherall. Demystifying 802.11n power consumption. In *HotPower*, 2010.
- [17] Vikram Iyer, Vamsi Talla, Bryce Kellogg, Shyamnath Gollakota, and Joshua Smith. Inter-technology backscatter: Towards internet connectivity for implanted devices. In *Proceedings of the 2016 ACM SIGCOMM Conference*, SIGCOMM ’16, pages 356–369, New York, NY, USA, 2016. ACM.
- [18] Bryce Kellogg. Passive wi-fi and interscatter. In *Proceedings of the 3rd Workshop on Hot Topics in Wireless*, HotWireless ’16, pages 22–22, New York, NY, USA, 2016. ACM.
- [19] Bryce Kellogg, Aaron Parks, Shyamnath Gollakota, Joshua R. Smith, and David Wetherall. Wi-fi backscatter: Internet connectivity for rf-powered devices. In *Proceedings of the 2014 ACM Conference on SIGCOMM*, SIGCOMM ’14, pages 607–618, New York, NY, USA, 2014. ACM.
- [20] Bryce Kellogg, Vamsi Talla, Joshua R. Smith, and Shyamnath Gollakot. Passive wi-fi: Bringing low power to wi-fi transmissions. *GetMobile: Mobile Comp. and Comm.*, 20(3):38–41, January 2017.
- [21] S. Keyrouz, H.J. Visser, and A.G. Tijhuis. Multi-band simultaneous radio frequency energy harvesting. In *Antennas and Propagation (EuCAP), 2013 7th European Conference on*, pages 3058–3061, 2013.
- [22] J. Kimionis, A. Bletsas, and J. N. Sahalos. Increased range bistatic scatter radio. *IEEE Transactions on Communications*, 62(3):1091–1104, March 2014.
- [23] J.G. Koomey, S. Berard, M. Sanchez, and H. Wong. Implications of historical trends in the electrical efficiency of computing. *Annals of the History of Computing, IEEE*, 33(3):46–54, 2011.
- [24] Vincent Liu, Aaron Parks, Vamsi Talla, Shyamnath Gollakota, David Wetherall, and Joshua R Smith. Ambient backscatter: wireless communication out of thin air. In *Proceedings of the ACM SIGCOMM 2013 conference on SIGCOMM*, pages 39–50. ACM, 2013.

- [25] Y. Liu, C. Huang, H. Min, G. Li, and Y. Han. Digital correlation demodulator design for RFID reader receiver. In *Wireless Communications and Networking Conference, 2007. WCNC 2007. IEEE*, pages 1664–1668. IEEE, 2007.
- [26] BR Mace. Wave reflection and transmission in beams. *Journal of Sound and Vibration*, 97(2):237–246, 1984.
- [27] K. Mimis, D. R. Gibbins, S. Dumanli, and G. T. Watkins. The ant and the elephant: ambient rf harvesting from the uplink. *IET Microwaves, Antennas Propagation*, 11(3):386–393, 2017.
- [28] Pavel V Nikitin, Shashi Ramamurthy, Rene Martinez, and KVS Rao. Passive tag-to-tag communication. In *RFID*, 2012.
- [29] P.V. Nikitin and K.V.S. Rao. Theory and measurement of backscattering from RFID tags. *Antennas and Propagation Magazine, IEEE*, 48(6):212 –218, december 2006.
- [30] K. Niotaki, S. Kim, S. Jeong, A. Collado, A. Georgiadis, and M.M. Tentzeris. A compact dual-band rectenna using slot-loaded dual band folded dipole antenna. *Antennas and Wireless Propagation Letters, IEEE*, 12:1634–1637, 2013.
- [31] A. N. Parks and J. R. Smith. Active power summation for efficient multiband rf energy harvesting. In *2015 IEEE MTT-S International Microwave Symposium*, pages 1–4, May 2015.
- [32] Aaron N. Parks, Angli Liu, Shyamnath Gollakota, and Joshua R. Smith. Turbocharging ambient backscatter communication. *SIGCOMM Comput. Commun. Rev.*, 44(4):619–630, August 2014.
- [33] A.N. Parks, A.P. Sample, Yi Zhao, and J.R. Smith. A wireless sensing platform utilizing ambient rf energy. In *Radio and Wireless Symposium (RWS), 2013 IEEE*, pages 331–333, 2013.
- [34] A.N. Parks and J.R. Smith. Sifting through the airwaves: Efficient and scalable multi-band rf harvesting. In *RFID (IEEE RFID), 2014 IEEE International Conference on*, pages 74–81, April 2014.
- [35] V. Pillai, H. Heinrich, D. Dieska, P.V. Nikitin, R. Martinez, and K.V.S. Rao. An ultra-low-power long range battery/pассивный RFID tag for UHF and microwave bands with a current consumption of 700 nA at 1.5 V. *Circuits and Systems I: Regular Papers, IEEE Transactions on*, 54(7):1500–1512, 2007.

- [36] R. Piyare, A. L. Murphy, C. Kiraly, P. Tosato, and D. Brunelli. Ultra low power wake-up radios: A hardware and networking survey. *IEEE Communications Surveys Tutorials*, PP(99):1–1, 2017.
- [37] J. Qian, F. Gao, G. Wang, S. Jin, and H. Zhu. Noncoherent detections for ambient backscatter system. *IEEE Transactions on Wireless Communications*, 16(3):1412–1422, March 2017.
- [38] X. Qing and N. Yang. A folded dipole antenna for RFID. In *Antennas and Propagation Society International Symposium, 2004. IEEE*, volume 1, pages 97–100. IEEE, 2004.
- [39] K.V.S. Rao, P.V. Nikitin, and S.F. Lam. Antenna design for UHF RFID tags: A review and a practical application. *Antennas and Propagation, IEEE Transactions on*, 53(12):3870–3876, 2005.
- [40] Mark A Richards, James A Scheer, and William A Holm. *Principles of Modern RADAR: Basic Principles*. Scitech, 2010.
- [41] A. Sample and J.R. Smith. Experimental results with two wireless power transfer systems. In *Radio and Wireless Symposium, 2009. RWS '09. IEEE*, pages 16–18, 2009.
- [42] Alanson P. Sample, Aaron N. Parks, Scott Southwood, and Joshua R. Smith. Wireless ambient radio power. In Joshua R. Smith, editor, *Wirelessly Powered Sensor Networks and Computational RFID*, pages 223–234. Springer New York, 2013.
- [43] A.P. Sample, D.J. Yeager, P.S. Powledge, A.V. Mamishev, and J.R. Smith. Design of an RFID-based battery-free programmable sensing platform. *IEEE Transactions on Instrumentation and Measurement*, 57(11):2608–2615, November 2008.
- [44] G. Seigneuret, E. Bergeret, and P. Pannier. Auto-tuning in passive uhf rfid tags. In *NEWCAS Conference (NEWCAS), 2010 8th IEEE International*, pages 181–184, 2010.
- [45] Joshua R Smith. Range scaling of wirelessly powered sensor systems. In *Wirelessly powered sensor networks and computational RFID*, pages 3–12. Springer New York, 2013.
- [46] H. Stockman. Communication by means of reflected power. *Proceedings of the IRE*, 36(10):1196–1204, Oct 1948.
- [47] Vamsi Talla, Mehrdad Hessar, Bryce Kellogg, Ali Najafi, Josh Smith, and Shyam Gol-lakota. Lora backscatter: Enabling the vision of ubiquitous connectivity.

- [48] S.J. Thomas and M.S. Reynolds. A 96 mbit/sec, 15.5 pj/bit 16-qam modulator for uhf backscatter communication. In *RFID (RFID), 2012 IEEE International Conference on*, pages 185–190, April 2012.
- [49] R.H. Walden. Analog-to-digital converter survey and analysis. *Selected Areas in Communications, IEEE Journal on*, 17(4):539 –550, apr 1999.
- [50] Chouchang Yang, Jeremy Gummesson, and Alanson Sample. Riding the airways: Ultra-wideband ambient backscatter via commercial broadcast systems. *Proceedings of IEEE INFOCOM*, 2017.
- [51] PENGYU ZHANG, Dinesh Bharadia, Kiran Joshi, and Sachin Katti. Enabling backscatter communication among commodity wifi radios. In *Proceedings of the 2016 ACM SIGCOMM Conference*, SIGCOMM ’16, pages 611–612, New York, NY, USA, 2016. ACM.